Atmos. Chem. Phys., 26, 12019–12036, 2026
https://doi.org/10.5194/acp-26-12019-2026

Atmospheric Chemistry and Physics
Open Access
EGU

Research article

Radiocarbon in atmospheric CH_4 and CO_2 at Jungfraujoch in 2019–2024: influence of regional nuclear emissions and current global atmospheric $^{14}CH_4$ signal

Thomas Laemmel[1,2,a], Dylan Geissbühler[1,2,b], Stephan Henne[3], Ryo Fujita[4], Heather Graven[5], Christophe Espic[1,2,c], Matthias Bantle[1], Negar Haghipour[6], Franz Conen[7], Dominik Brunner[3], Martin Steinbacher[3], Giulia Zazzeri[8], Samuel Hammer[9], Markus Leuenberger[2,10], and Sönke Szidat[1,2]

[1]Department of Chemistry, Biochemistry and Pharmaceutical Sciences, University of Bern, Bern, Switzerland
[2]Oeschger Centre for Climate Change Research, University of Bern, Bern, Switzerland
[3]Empa, Swiss Federal Laboratories for Materials Science and Technology, Dübendorf, Switzerland
[4]Meteorological Research Institute, Japan Meteorological Agency, Tsukuba, Japan
[5]Department of Physics, Imperial College London, London, United Kingdom
[6]Department of Earth and Planetary Sciences and Laboratory of Ion Beam Physics, ETH Zurich, Zurich, Switzerland
[7]Department of Environmental Sciences, University of Basel, Basel, Switzerland
[8]Ricerca sul Sistema Energetico – RSE S.p.A., Milan, Italy
[9]Institute of Environmental Physics, Heidelberg University, ICOS-CRL, Heidelberg, Germany
[10]Climate and Environmental Physics, University of Bern, Bern, Switzerland
[a]now at: WANNER Expert GmbH, Solothurn, Switzerland
[b]now at: Institute for Marine and Atmospheric Research Utrecht, Utrecht University, Utrecht, the Netherlands
[c]now at: MIRO Analytical AG, Wallisellen, Switzerland

Correspondence: Thomas Laemmel (thom.laemmel@gmail.com) and Sönke Szidat (soenke.szidat@unibe.ch)

Received: 17 January 2026 – Discussion started: 11 February 2026
Revised: 27 May 2026 – Accepted: 4 August 2026 – Published: 24 August 2026

Abstract. Radiocarbon (^{14}C) is a valuable tracer to determine the relative fossil fractions of emitted carbonaceous greenhouse gases, such as CO_2 and CH_4. While atmospheric $\Delta^{14}CO_2$ measurements have been conducted at multiple sites for several decades, $\Delta^{14}CH_4$ measurements remain more limited, mainly due to measurement challenges. In addition, $^{14}CH_4$ emissions from nuclear power plants (NPPs) can complicate data interpretation. In this study, fortnightly $\Delta^{14}CH_4$ and $\Delta^{14}CO_2$ measurements at the Swiss High-Altitude Research Station Jungfraujoch (JFJ, about 3500 m a.s.l.) between 2019 and 2024 are presented. Over this period, $\Delta^{14}CH_4$ values showed an increase from 350 ± 19 ‰ to 381 ± 13 ‰, while $\Delta^{14}CO_2$ values decreased from -2.0 ± 3.8 ‰ to -12.7 ± 2.0 ‰, respectively. The former is related to the slight increase of $^{14}CH_4$ emissions from the nuclear industry over the last years, while the latter is linked to the continued dilution of the $^{14}CO_2$ signal due to the release of ^{14}C-devoid CO_2 from combustion of fossil fuels. Despite its high elevation, JFJ is still influenced by NPPs operating in Europe. To assess the nuclear ^{14}C contribution to our individual measurements, we use a combination of in situ ^{222}Radon measurements and Lagrangian particle dispersion model convolved with bottom-up inventory of ^{14}C emissions from NPPs. Furthermore, our $\Delta^{14}CH_4$ measurements reasonably agree with simulated atmospheric values of $\Delta^{14}CH_4$ estimated by a global atmospheric one-box model and an estimation of global nuclear $^{14}CH_4$ emissions.

Published by Copernicus Publications on behalf of the European Geosciences Union.

1 Introduction

Carbon dioxide (CO_2) and methane (CH_4) are the two main anthropogenic greenhouse gases (GHGs) responsible for global climate change (IPCC, 2023; WMO, 2025). Since the Industrial Revolution around 1850, their global atmospheric concentrations have been multiplied by about 1.5 and 2.7, respectively, from around 285 to 422.8 ppm in 2024 for CO_2 (Etheridge et al., 1996; Lan et al., 2025b) and from around 800 to 1930 ppb in 2024 for CH_4 (Lan et al., 2025a; MacFarling Meure et al., 2006). Anthropogenic emissions of CO_2 and CH_4 (mainly from the energy sector for fossil CO_2 and CH_4, and agriculture and waste management for biogenic CH_4) are responsible for this rise in concentrations and resulting climate change. In the period 2010–2019, CO_2 and CH_4 were responsible for a global warming of around 0.8 and 0.5 °C, respectively, relative to the period 1850–1900 (IPCC, 2023). To implement effective mitigation measures, the main emission sources of both GHGs have to be better quantified and monitored.

Radiocarbon (^{14}C), a radioactive isotope of carbon with a half-life of 5700 ± 30 years (Kutschera, 2013; Roberts and Southon, 2007), is a valuable tracer to distinguish fossil from modern carbon sources. Naturally produced in the upper atmosphere through the interaction of thermal neutrons with nitrogen, ^{14}C is finally oxidized to $^{14}CO_2$, which can be integrated into the biosphere via photosynthesis and into the hydrosphere via gas exchange at the water-atmosphere interface (Graven et al., 2020). On the one hand, fossil fuels (e.g. coal, oil, natural gas) that were formed millions of years ago are now devoid of ^{14}C because of its short half-life compared to geological time scales. On the other hand, CO_2 and CH_4 derived from fresh organic matter contain ^{14}C / ^{12}C ratios close to the current atmospheric $^{14}CO_2$ signature. Atmospheric $^{14}CO_2$ and $^{14}CH_4$ measurements are thus valuable proxies to study the different sources of CO_2 and CH_4 released to the atmosphere.

Atmospheric $^{14}CO_2$ measurements have a long history. Since the first measurements focused on the documentation of the atmospheric $^{14}CO_2$ bomb peak in the 1950s–1960s associated with nuclear bomb tests (Levin et al., 1985; Manning et al., 1990; Nydal and Lövseth, 1983; Rafter and Fergusson, 1957), there are now international monitoring programs following the long-term evolution of atmospheric $^{14}CO_2$ at background sites (e.g., Hammer et al., 2017; Turnbull et al., 2007). Observations at the High-Altitude Research Station Jungfraujoch (JFJ) in Switzerland have been conducted since 1986; there, two-weeks integrated CO_2 samples have been collected and further purified and analyzed at the Heidelberg laboratory (Germany) (Levin et al., 2013, 2023). On a more local scale, atmospheric $^{14}CO_2$ measurements have been used to study CO_2 emissions from urban areas to entire countries (Basu et al., 2020; Graven et al., 2018; Levin et al., 2003). Since the bomb peak in the middle of the last century, $\Delta^{14}CO_2$ values have been declining by the dilution of the enriched atmospheric ^{14}C signal in both land and ocean carbon sinks and by the emissions of ^{14}C-free fossil fuel CO_2, which depletes the atmospheric $\Delta^{14}CO_2$ signal (Graven et al., 2024; Oeschger et al., 1975).

Atmospheric measurements of $^{14}CH_4$ have been more limited than $^{14}CO_2$ so far. One reason for this is related to the about 200-times lower atmospheric CH_4 concentration compared to CO_2: while 2–5 L of air are sufficient to analyze $^{14}CO_2$ (e.g. yielding about 1 mgC from 5 L air at 420 ppm CO_2), several tens of liters are required for $^{14}CH_4$ analysis (e.g. yielding about 50 µgC from 50 L air at 2 ppm CH_4). The sampling and analysis of $^{14}CH_4$ is therefore difficult, and prone to CO_2 contamination. Besides this technical consideration, the interpretation of atmospheric $^{14}CH_4$ measurements may be complicated at study sites that are influenced by nuclear power plants (NPPs) (Eisma et al., 1994, 1995; Levin et al., 1992). Pressurized water reactors (PWRs), which are currently the most widely operated plants (IAEA PRIS, 2025), emit ^{14}C mainly as $^{14}CH_4$, whereas other reactor types emit ^{14}C mainly as $^{14}CO_2$ (Vance et al., 1995; Zazzeri et al., 2018). The annual global nuclear ^{14}C emission rate for 2016 has been estimated to about 105 TBq for $^{14}CO_2$ and about 45 TBq for $^{14}CH_4$ (Zazzeri et al., 2018). Although $^{14}CO_2$ emissions are larger, the influence of nuclear $^{14}CH_4$ emissions on atmospheric $^{14}CH_4$ is stronger due to the much lower atmospheric CH_4 concentration compared to CO_2. This also explains why current atmospheric ^{14}C / ^{12}C ratios are about 35 % higher for $^{14}CH_4$ than $^{14}CO_2$ (Emmenegger et al., 2025a; Gonzalez Moguel et al., 2022).

Despite these challenges, several analysis setups and atmospheric $^{14}CH_4$ datasets have been reported from ice cores and atmospheric samples. Pioneering atmospheric $^{14}CH_4$ measurements were reported by Lowe et al. (1988) and Wahlen et al. (1989). In the 1990s, Levin et al. (1992) reported the first sporadic $^{14}CH_4$ measurements between 1988 and 1991 at JFJ. Eisma et al. (1994, 1995) measured atmospheric $^{14}CH_4$ values from a tall tower in the Netherlands and highlighted the challenge to interpret $^{14}CH_4$ measurements, even when using an atmospheric transport model to evaluate the nuclear influence on the measurements. Lassey et al. (2007a, b) compiled more than 200 individual atmospheric $^{14}CH_4$ measurements from the Northern and Southern Hemispheres between 1986 and 2000 and deduced that about 30 % of the global CH_4 source for this period had a fossil origin. Hmiel et al. (2020) used $^{14}CH_4$ measurements from ice cores to better constrain natural geological (i.e., fossil) CH_4 emissions during the preindustrial era. By synthetizing atmospheric CH_4 concentration and its major isotopologues ($^{13}CH_4$, CH_3D and $^{14}CH_4$) for 1750–2015, Fujita et al. (2025) estimated 30 % lower global CH_4 emissions from the fossil-fuel industry compared to previous isotope-based studies relying mostly on CH_4 and $^{13}CH_4$ without ^{14}C consideration. Another output of their work was an updated inventory of the nuclear $^{14}CH_4$ emissions between 1960 and 2015 based on nuclear electricity production data.

In recent years, several novel analysis systems and studies for $^{14}CH_4$ have been reported (Espic et al., 2019; Gonzalez Moguel et al., 2022; Zazzeri et al., 2021, 2023) increasing the analysis capabilities, even in a more field-compatible way (Zazzeri et al., 2025). Despite these new studies, recent background atmospheric $^{14}CH_4$ values are still missing. At the Laboratory for the Analysis of Radiocarbon with AMS (LARA, University of Bern) (Szidat, 2020), a system exists since 2019 to analyze $^{14}CH_4$ and $^{14}CO_2$ from a single atmospheric sample (Espic et al., 2019) and was already used in several studies (Espic et al., 2025; Etiope et al., 2024; Zazzeri et al., 2025). Here, we present atmospheric $^{14}CH_4$ and $^{14}CO_2$ measurements conducted at the High-Altitude Research Station Jungfraujoch between 2019 and 2024, discuss their representativeness regarding the nuclear influence in Europe and show their relevance as worldwide background values.

2 Material & Methods

2.1 Jungfraujoch Site and Sampling Strategy

The High-Altitude Research Station Jungfraujoch (stretching from 3455 to 3585 m a.s.l., 46°32′51″ N, 7°59′7″ E, JFJ), established in 1931, is located on a mountain ridge in the Swiss Alps. Among others, this station is part of the Global Atmosphere Watch (GAW) network as well as of the Network for the Detection of Atmospheric Composition Change (NDACC). Furthermore, JFJ is labelled as a Class 1 Station of the European-wide Integrated Carbon Observation System (ICOS) Research Infrastructure (Heiskanen et al., 2022) since May 2018 (Yver-Kwok et al., 2021). Because of its high elevation, JFJ is a well-recognized international background station (Leuenberger and Flückiger, 2008). However, it is also intermittently impacted by direct transport from the polluted planetary boundary layer, most frequently during daytime from April to September (Henne et al., 2010).

A fortnightly air sampling program measuring $^{14}CH_4$ and $^{14}CO_2$ at JFJ every two weeks started in January 2019. Until March 2023, two morning grab air samples were taken using a membrane pump (N022AN.18, KNF Neuberger AG, Germany) that directly pumped air from the Sphinx terrasse (3580 m a.s.l.) at JFJ into two PE-Al-PE 120 L bags (Tecobag, Tesseraux Spezialverpackungen GmbH, Germany) through a dedicated sampling line (Synflex Decabon 1300 Tubing, OD = 6 mm). The sampled air was dried with a magnesium perchlorate dryer ($Mg(ClO_4)_2$, ACS reagent, ThermoFisher, USA) to avoid condensation and further reactions between water vapor and other sampled gas species. The sampling duration per bag was commonly between 20 and 55 min depending on the ambient pressure, temperature and the flow resistance during sampling due to the dryer and the long length and small diameter of the sampling line. The morning grab samplings were performed manually and as early as possible in the morning to avoid the influence of the daytime planetary boundary layer; in practice, it commonly occurred between 07:00 and 10:00 UTC (i.e., 08:00 and 12:00 local time, UTC+1/UTC+2), depending on the seasonal train schedule ensuring the public transport up to JFJ.

To increase the reproducibility of the air sampling procedure and its representativeness as a background measurement, an automated air sampling system was developed replacing the manual sampling from 18 April 2023 onwards (Fig. 1). Its development was guided by two principles: (1) air sampling should be restricted to nighttime when the station mostly resides within the free troposphere, allowing for the collection of temporally integrated samples over multiple days; and (2) air sampling should occur as far as possible passively, i.e., without any mechanical pumps in contact with the sampled air, thereby minimizing the risk of contamination from membrane outgassing. The novel Jungfraujoch Air Sampling System (JASS) consisted of a custom-made electropolished steel sampling tank (volum = 260 L, length (L) = 140 cm, outer diameter (OD) = 51 cm, Bechtiger Edelstahl AG, Switzerland) coupled to a sampling box containing a series of valves, all controlled by a home-made control unit including a Raspberry Pi 4B module (Raspberry Pi Ltd, United Kingdom) (Fig. 1). The whole system was installed under the roof of the research station at JFJ, at about 3462 m a.s.l. (Fig. S1 in the Supplement). Its design allows a routine integrated nighttime air sampling procedure lasting 6 h every night (between 00:00 and 06:00 UTC) over 14 d, so integrating 84 h in total. Compared to the initial fortnightly morning grab sampling strategy, integrated sampling gives a more representative air mixture for every two-week period of interest (Fig. S2).

The inlet of the sampling line (Synflex Decabon 1300 Tubing, OD = 12 mm, $L \sim 10$ m) was protected by a dust filter (Fig. 1). A flushing membrane pump (N022AN.18, KNF Neuberger AG, Germany) continuously conveyed outside air through this sampling line and a water separator to the sampling box. Through two T-pieces (SS-12M0-3, Swagelok, USA) integrated in this sampling line, part of the sampled air could be further directed into the sampling box, either automatically using line (1), or manually using line (2) (Fig. 1). At the beginning of a sampling period, the tank was evacuated using a vacuum pump (MV 2 NT, Vacuubrand GmbH + Co KG, Germany); the end pressure was $\leq$ 0.7 mbar. During automatic air sampling, the sampling line (1) was open and worked as follows: both 2/2-way solenoid valves A1 and A2 (0330-A-02, Bürkert, Germany) were open and the 3/2-way solenoid valve B (0330-F-02, Bürkert, Germany) was in the position connecting this line with the tank (blue connection, Fig. 1); the mass-flow controller (MFC, F-201DV, Bronkhorst, The Netherlands) between A1 and A2 ensured a controlled air flow into the system and the increasing pressure in the tank was monitored by a pressure gauge (RPT 200 AR, Pfeiffer Vacuum, Germany); in front of the MFC, a $Mg(ClO_4)_2$ dryer dried the sampled air and a 0.5 µm filter (SS-4FWS-05, Swagelok, USA) protected the MFC from

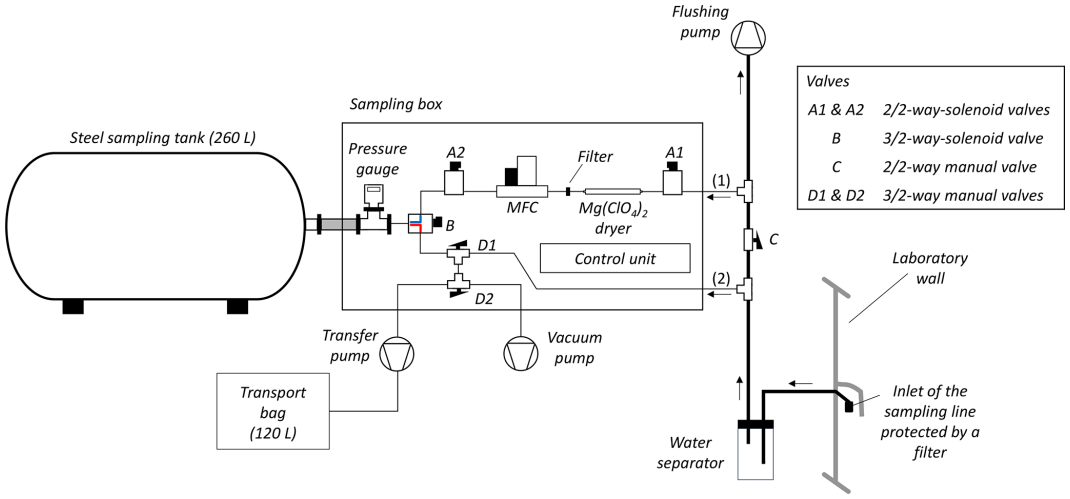

Figure 1. Jungfraujoch Air Sampling System (JASS) used for integrated nighttime air sampling over 14 d since 18 April 2023.

particulate matter. After 6 h of sampling, both A1 and A2 valves were closed. This sampling procedure was repeated every night. After 14 nighttime samplings, the pressure in the tank reached 600–650 mbar. The mean ambient atmospheric pressure at JFJ was 656 mbar over the period 2019–2024 (Emmenegger et al., 2025d); we configured our passive sampling system in a way where the tank pressure was always lower than ambient pressure, otherwise the passive sampling based on the pressure difference between the tank and the ambient pressure would not work. On-site, the transfer of the sampled air from the tank into a new bag was prepared in this manner: a dedicated transfer pump (N922SPE, KNF Neuberger AG, Germany) was turned on and the manual 3/2-way valve D2 was turned to the left (Fig. 1); the position of the 3/2-way valve D1 stayed by default turned to the left. The Python script running on the Raspberry Pi was then restarted to turn on the vacuum pump and switch the 3/2-way solenoid valve B in the position connecting the tank with the pump line (red connection, Fig. 1). At this stage, the transfer pump was evacuating the tank and after ~ 30 s of line flushing, a bag was connected to the line for the transfer of the sampled air. After about one hour, enough air was transferred to the bag for further ^{14}C analyses. It was then closed and disconnected from the transfer pump (tank pressure at around 70–90 mbar). To accelerate the evacuation of the tank and condition it again for the next sampling, the valve D2 was then turned to the right, and the vacuum pump was evacuating the tank. The system was left like this for the rest of the day and, at 23:59 UTC, valve B switched automatically back to its sampling position (blue connection, Fig. 1) (final tank pressure ≤ 0.7 mbar), the vacuum pump turned off and the whole system was ready to start the next sampling period. The whole sampling system was validated to be leak-tight in our laboratory in Bern before being transferred to JFJ. The low pressure achieved in the tank before each new sampling every two weeks regularly validated the tightness of the sampling system.

2.2 Sample preparation and measurements of $\Delta^{14}CH_4$ and $\Delta^{14}CO_2$

For both morning grab and integrated nighttime sampling strategies, the air collected in bags was transferred to the LARA laboratory at the University of Bern (Szidat, 2020), where a dedicated extraction line for $^{14}CH_4$ and $^{14}CO_2$ analysis was available (see Espic et al., 2019 for details). The extraction was generally done within one week after sampling and most of the time the day after. The typical air volume for one analysis was 60 L. During a preconcentration step, this air was pumped successively through three traps filled either with fiber glass or activated charcoal and cooled down with liquid nitrogen; this allowed us to preserve the whole amount of CH_4 contained in the initial 60 L of air by trapping or pumping away the main other gas species, especially nitrogen and oxygen. CO_2 was quantitatively trapped in the first trap and could be collected separately (see below). After that, the gas sample volume was about 10 mL, small enough to be run through a gas chromatograph (GC, 7890B, Agilent, USA; ShinCarbon ST 80/100 packed column; thermal conductivity detector, He as carrier gas) to purify the sample. CH_4 was isolated quantitatively from the remaining CO and CO_2 present in trace quantities due to different elution times in the GC (CO: ~ 2 min; CH_4: ~ 8 min; CO_2: ~ 13 min). Downstream of the GC, the extracted pure CH_4 was converted into CO_2 by combustion in a flow oven at 950 °C using copper oxide wires as a catalyst. The CH_4-derived CO_2 (~ 60 to 70 µg of carbon, µgC) was transferred into glass ampoules (OD $=$ 4 mm) and sealed for gas radiocarbon measurements. After the CH_4 extraction procedure, the CO_2 of the sample held in the first trap was recovered by cryogenic transfer into a ~ 55 mL glass flask. The car-

bon mass of the recovered CO_2 was typically greater than 1 mgC, which was transformed into graphite using an automated graphitization equipment (AGE) (Němec et al., 2010). Concerning the quality control of the $^{14}CH_4$ extraction system, Espic et al. (2019) reported a cross-contamination of 0.4 ± 0.2 % ($n = 2$) from the previous sample and an extraction yield of 101.2 ± 1.4 ($n = 13$).

Radiocarbon analyses of the gaseous CH_4-derived CO_2 samples and the graphite CO_2 samples were performed either at LARA or at the Laboratory of Ion Beam Physics, ETH Zürich, Switzerland, using the same type of AMS (MIni CArbon DAting System, MICADAS), equipped with a gas ion source (Ruff et al., 2007; Synal et al., 2007). Glass ampoules were cracked in a dedicated gas inlet system (Wacker et al., 2013) and the CH_4-derived CO_2 was diluted with He to ~ 5 %, transferred into a syringe, and then fed into the ion source using a constant gas flow. Graphite samples were introduced directly to the MICADAS source. For both types of samples, raw $^{14}C / ^{12}C$ as well as $^{13}C / ^{12}C$ ratios were converted into $F^{14}C$ and $\delta^{13}C$ values, respectively, by performing a blank subtraction as well as a standard normalization and correction for isotope fractionation (only for $F^{14}C$) using ^{14}C-free CO_2 (Blank) ($F^{14}C = 0$) and CO_2 produced from the primary NIST standard oxalic acid II (OX-II) (SRM 4990C) ($F^{14}C = 1.34066$, $\delta^{13}C = -17.8$ ‰), respectively. For the gas measurements, standards came from two gas bottles directly attached to the gas inlet system; both mixtures consisted of 5 % CO_2 with the $F^{14}C$ value of interest and 95 % He. For the graphite measurements, both standards underwent the same sample preparation as the CO_2 samples and were measured with them in the same magazine. Gas samples were commonly measured starting with 2–4 OX-II and 2 Blank standards, then with the samples in chronological sampling order and finishing with 2–4 OX-II and 2 Blank to account for potential drifts. The dataset presented here was built over 40 measurement days in 6 years. Per measurement day, about 24–32 standards and samples, including about 5–8 from JFJ, were measured; the remaining samples came from other sampling sites or further projects. The average standard deviation of all the OX-II standards used for normalization within a single measurement day was ± 0.007 (in $F^{14}C$) whereas the average single OX-II precision derived from counting statistics was ± 0.010 ($n = 204$). Graphite samples were generally measured in a 39-position magazine containing 3–4 OX-II and 3 Blank samples. The dataset presented here was built over 35 magazines. The average standard deviation of all the OX-II standards used for normalization within a single measurement day was ± 0.0018 (in $F^{14}C$) whereas the average single OX-II precision derived from counting statistics was ± 0.0025 ($n = 117$). The final data evaluation was done using the BATS tool (Wacker et al., 2010). The typical measurement precision is 8 ‰ for $^{14}CH_4$ and 1.5 ‰ for $^{14}CO_2$ (see below). Throughout the current work, ^{14}C results are reported using the notation $\Delta^{14}C$, and calculated with age correction as the parameter Δ in Stuiver and Polach (1977).

2.3 Ancillary measurements and datasets

At JFJ, in the framework of the ICOS measurement program, CO_2 and CH_4 concentrations are measured continuously using cavity ringdown spectroscopy; corresponding hourly average values were used in the present study (Emmenegger et al., 2025b, c). These values were used, among other purposes, to determine the stability of CH_4 and CO_2 concentrations in the transfer bags between sampling and extraction. CH_4 and CO_2 concentrations were measured in the remaining sampled air after extraction with a cavity ringdown spectrometer (Picarro G2401, Picarro Inc., USA) calibrated with three gas bottles with known CH_4 and CO_2 concentrations (1861.2, 1955.9, and 2206.7 ppb for CH_4; 379.21, 418.38, and 458.62 ppm for CO_2) (Carbagas, Switzerland). Mean differences between concentrations measured after extraction and measured in situ were 1.3 ± 2.8 ppb and 0.7 ± 1 ppm, for CH_4 and CO_2, respectively ($n = 13$, between January and July 2024).

Furthermore, integrated samples have been collected at JFJ since 1986 to analyze atmospheric $\Delta^{14}CO_2$, first started by the University of Heidelberg, now run as part of the ICOS Research Infrastructure (Emmenegger et al., 2025a; Hammer et al., 2017; Levin and Kromer, 2004). The dedicated setup draws ambient air throughout 14 d through a sodium hydroxide solution, in which CO_2 is chemically absorbed. We chose the same 14 d schedule for our nighttime sampling as the ICOS schedule to enable a comparison between both datasets. ICOS $\Delta^{14}CO_2$values are also reported as Δ values according to Stuiver and Polach (1977). Furthermore, atmospheric $\Delta^{14}CO_2$ values from the Mace Head Atmospheric Research Station (MHD, Ireland) are used here for comparison (Hammer and Levin, 2023); due to its location exposed to westerly winds from the North Atlantic Ocean, MHD is often used as European background station.

We also made use of continuous ^{222}Radon (in the following referred as Rn) measurements at JFJ with a two-filter dual loop alpha particle detector, operated by the University of Basel since 2009 (Griffiths et al., 2014) and which is meanwhile part of ICOS (Fig. S1). Rn is emitted from land surfaces into the atmosphere and because of its half-life of 3.8 d, it is a potential tracer of recent land contact. In this study, Rn was used as a proxy to distinguish free tropospheric samples from those originating from the planetary boundary layer (i.e., with recent land contact). To account for variations in ambient temperature and pressure, the raw hourly Rn concentrations (Conen, 2025) were converted into Rn values at STP conditions (i.e., $T = 0$ °C, $P = 101\,325$ Pa).

To evaluate the accuracy and stability of our $\Delta^{14}CH_4$ and $\Delta^{14}CO_2$ measurements over time, regular measurements of a pressurized air bottle (PAB) (Carbagas, Switzerland) considered as an internal standard have been performed

since March 2022 in parallel to the measurements of the JFJ samples; this air strictly underwent the same extraction and measurement procedures as the JFJ samples, commonly just before them. A first bottle was measured until end of July 2023 ($CH_4 = 1997 \pm 2$ ppb, and $CO_2 = 434.5 \pm 0.1$ ppm), replaced by a second one in August 2023 ($CH_4 = 2178 \pm 2$ ppb, and $CO_2 = 455.8 \pm 0.1$ ppm). It should be noted that the $\Delta^{14}CH_4$ and $\Delta^{14}CO_2$ values of both bottles were a priori unknown and that we used them to evaluate the stability of the values derived from our measurement procedure.

2.4 Atmospheric modeling of nuclear ^{14}C influence at JFJ

One goal of the present study was to evaluate the influence of nuclear $^{14}CH_4$ and $^{14}CO_2$ emissions on our atmospheric $\Delta^{14}CH_4$ and $\Delta^{14}CO_2$ measurements at JFJ. For this purpose, the amount and transport of $^{14}CH_4$ and $^{14}CO_2$ molecules from nuclear emissions were simulated using the Lagrangian particle dispersion model FLEXible PARTicle (FLEXPART) (Pisso et al., 2019) in the version adopted for inputs from the numerical weather prediction model COSMO (Henne et al., 2016). Here, we use the COSMO analysis product of the Swiss Federal Office of Meteorology and Climatology (MeteoSwiss), based on high spatial resolution ($1\,km \times 1\,km$) model simulations and using a local ensemble transform Kalman filter (LETKF) meteorological data assimilation system (Schraff et al., 2016). Meteorological analysis fields from this product were available at 1 h temporal resolution for the Alpine domain (approximately 0–17° E, 42–50° N). The FLEXPART-COSMO model was used in previous atmospheric studies including the verification of the Swiss CH_4 emission inventory (Henne et al., 2016), the influence of nuclear $^{14}CO_2$ emissions on $\Delta^{14}CO_2$ at a Swiss tall tower (Berhanu et al., 2017), the analysis of CO_2 and $\delta^{13}CO_2$ at JFJ (Pieber et al., 2022), and for inverse modeling of halocarbon emissions over Switzerland (Katharopoulos et al., 2023). Here, the model was operated in the same way as in Katharopoulos et al. (2023). In short, 50 000 model particles were released continuously from JFJ for every 3 h interval and traced backwards in time for 4 d or until they reached the domain boundaries. Afterwards, the integration of the particles' path was continued for up to 10 d in a European scale FLEXPART-IFS simulation driven by hourly inputs from the European Centre for Medium-Range Weather Forecasts (ECMWF) HRES operational forecast/analysis product available at $0.1° \times 0.1°$ resolution. The residence time of particles below a height of 50 m above model ground is then estimated in 3 h intervals and divided by air density provides so called source sensitivities (or concentration footprints).

Nuclear ^{14}C emissions between 2019 and 2023 from the nuclear power plants (NPPs) located in the modeling area (Fig. S3) were mostly estimated using the compilation of nuclear ^{14}C emissions of Laemmel et al. (2025). The atmospheric transport modeling was performed only for the period 2019–2023, as the input parameters for 2024 were not yet fully available. For most countries (i.e. Bulgaria, the Czech Republic, Romania, Slovakia, Slovenia, Spain, the Netherlands, and the United Kingdom) only annual total ^{14}C emissions for the NPPs were available. For some countries, more detailed information could be used including quarterly ^{14}C emissions from NPPs in France and Germany and monthly emissions for the Swiss NPPs Leibstadt and Gösgen, the Swedish NPPs Forsmark, Oskarshamn, and Ringhals, some NPPs in the United Kingdom and the French nuclear fuel reprocessing plant (NFRP) La Hague. Monthly inorganic and organic ^{14}C emissions from the Hungarian NPP Paks were also available for 2019 in this dataset. In addition to these published values, monthly inorganic and organic ^{14}C emissions for 2020–2023 were kindly made available by the operating company of the NPP Paks for this simulation. Reported emissions from the NPPs located in Belarus, Belgium, Russia, and Ukraine were not available; we estimated the annual ^{14}C emissions for each of these plants by multiplying the annual electricity production (Laemmel and Szidat, 2025) by reactor-specific emission factors (EF) of 0.19, 0.41, and $1.3\,TBq\,GWa^{-1}$ (GWa = gigawatt × 1 year) for PWR, VVER (water-cooled water-moderated energy reactor), and LWGR (light water graphite reactor), respectively. EF values for PWR and VVER were derived from the work of Fujita et al. (2025) and EF value for LWGR from the work of Zazzeri et al. (2018).

In a further step, $^{14}CH_4$ and $^{14}CO_2$ emissions per NPP were derived, as the reported values were mainly for total ^{14}C. We used data for inorganic and organic ^{14}C emissions that were reported in some countries (e.g., for NPPs in Germany, Hungary, Spain, Sweden, and Swizerland). For other countries we assumed that PWRs and VVERs emit 75 % of the total ^{14}C amount in organic form (so 25 % in inorganic form) and that all the other reactors (e.g. boiling water reactor (BWR), LWGR, and pressurized heavy water reactor (PHWR)) emit ^{14}C entirely in inorganic form, as also was assumed by Fujita et al. (2025). Furthermore, we assumed that the inorganic ^{14}C form is entirely composed of $^{14}CO_2$ and that $^{14}CH_4$ represents 72.5 % of the organic ^{14}C form; this last value was derived from the study of Kunz (1985) who analysed the composition of hydrocarbons of gaseous effluents at two PWRs in the USA. They reported values of 68 % and 77 % at the PWR Ginna and PWR Indian Point, respectively. Finally, the annual, quarterly or monthly emission amount of $^{14}CO_2$ and $^{14}CH_4$ available for each plant was equally divided into three-hour intervals to compute an emission rate per output step of the FLEXPART transport simulation. FLEXPART-derived source sensitivities, convolved with these emission rates yield ^{14}C mole fractions at the sampling site and a final nuclear correction $\Delta^{14}C^{Nuc}$ can be calculated assuming a mass balance model for C and ^{14}C (Graven et al., 2019) (See detailed equations in the Supplement).

2.5 Background atmospheric $\Delta^{14}CH_4$ modeling

Another goal of the present study was to evaluate the representativeness of our atmospheric $\Delta^{14}CH_4$ measurements at JFJ on a global level. For this goal, we compared our data with calculated atmospheric $\Delta^{14}CH_4$ values from a one-box model developed by Fujita et al. (2025). In this study, we extended their simulation until 2024 (Fig. S4) by updating their posterior CH_4 emission scenarios since 2013 (i.e., average of posterior CEDS, EDGARv5, and EDGARv6 scenarios; see Fujita et al., 2025). The anthropogenic CH_4 emissions for 2013–2022 were extended by using EDGARv8 (European Commission Joint Research Centre, 2023). To match the consistency with the posterior anthropogenic biogenic (BIO) and fossil fuel (FF) emissions in Fujita et al. (2025), the mean differences between EDGARv8 and Fujita et al. (2025) were calculated for 2008–2012 (BIO: 2.1 Tg yr^{-1}, FF: 9.8 Tg yr^{-1}) and then added to the values of EDGARv8 after 2013, respectively. For 2023–2024, the emissions of the Shared Socioeconomic Pathways (SSPs) were used. Here, we adopted SSP5-8.5 scenario in 2030 (Gidden et al., 2019) and linearly interpolated it between the EDGARv8 2022 emissions and the 2030 scenario emissions to the years 2023 and 2024. Natural biogenic CH_4 emissions were optimized based on the CH_4 mass balance equation to keep the consistency between our simulations and observed global mean CH_4 mole fractions by NOAA/GML (Lan et al., 2025a). To evaluate the ^{14}C signature of the biospheric CH_4 sources, $\Delta^{14}CO_2$ values for the time period 2013–2024 were derived from the SSP5-8.5 scenario (Graven et al., 2020). To extend the nuclear $^{14}CH_4$ emissions beyond 2013, we considered the posterior annual nuclear $^{14}CH_4$ emissions derived by Fujita et al. (2025). Assuming that only PWRs and VVERs are emitting $^{14}CH_4$, a mean annual emission factor Φ (GBq GWa^{-1}) was computed by dividing these emissions by the annual total electricity production by PWRs and VVERs derived from the data compilation by Laemmel and Szidat (2025). Considering the years 2008–2012, the mean Φ value was 250 GBq GWa^{-1}, the min Φ value was 243 GBq GWa^{-1}, and the max Φ value was 259 GBq GWa^{-1}. Considering these three Φ values and the annual total electricity production by PWRs and VVERs in 2013–2024 (the value for 2024 was chosen equal to 2023 as the real value was not yet available), three projections of annual nuclear $^{14}CH_4$ emissions were computed and used as variable input parameter in three different simulations of global atmospheric $\Delta^{14}CH_4$ values (Fig. S4g). Posterior geologic emissions, biospheric turnover time, total CH_4 lifetime, carbon and hydrogen kinetic isotope effects, and carbon and hydrogen CH_4 isotopic signatures for respective sources in Fujita et al. (2025) were repeated by the values in 2012 over 2013–2024.

The simulated $\Delta^{14}CH_4$ values were compared to our annual mean $\Delta^{14}CH_4$ values at JFJ for 2019–2024 and previously reported measurements from samples (ice cores and/or firn air) of Greenland and Antarctica (Hmiel et al., 2020) and from atmospheric samples (Gonzalez Moguel et al., 2022; Lassey et al., 2007b; Levin et al., 1992; Quay et al., 1999; Sparrow et al., 2018; Townsend-Small et al., 2012; Wahlen et al., 1989). Note that the data in Hmiel et al. (2020) was used in Fujita et al. (2025) as observational constraints. Several other studies were found but not used here because of the large scatter in the reported data (Lowe et al., 1988; Manning et al., 1990) or difficulties in the unit conversion into current radiocarbon parameters (Ehhalt, 1974).

3 Results

3.1 $\Delta^{14}CH_4$ measurements at Jungfraujoch

$\Delta^{14}CH_4$ values at JFJ between 2019 and 2024 were between 322 ‰ and 767 ‰ and showed a slightly increasing trend over the last six years (Fig. 2a, b). Some exceptionally high $\Delta^{14}CH_4$ values were measured (i.e., on 13 June and 25 July 2019; 13 May, 10 June and 24 June 2020; 12 May 2021) and were attributed to local and strong nuclear $^{14}CH_4$ releases. Rn values were lower than 5 Bq m^{-3} over 2019–2024 with generally lower values during winter months compared to summer months (Fig. 2c), which is consistent with a potentially stronger influence of the planetary boundary layer in summer. Annual mean CH_4 concentrations increased from 1930 ppb in 2019 to 1996 ppb in 2024 (Fig. 2d). Rn and CH_4 concentration data shown here represent the corresponding average values during the sampling intervals.

Reduced scatter in $\Delta^{14}CH_4$ values since the installation of the JASS in April 2023 is visible (Fig. 2a, b). Also, hourly Rn and CH_4 concentrations averaged over the JASS sampling periods show less amplitude variation after this date. For both parameters, corresponding values are closer to the monthly means measured in situ by the ICOS instruments (blue curves in Fig. 2c, d). The temporal stability of our $\Delta^{14}CH_4$ measurements from March 2022 onwards is evaluated using the regular $\Delta^{14}CH_4$ measurements of our two internal standard PAB bottles. The standard deviation of the $\Delta^{14}CH_4$ value for all 40 CH_4 measurements over 15 months for each PAB bottle (so about 80 CH_4 measurements in total) is 8 ‰ (Fig. S5a, b), which is lower than the instrumental uncertainty of a single $\Delta^{14}CH_4$ measurement (12 ‰) indicating the satisfactory long-term reproducibility of our $\Delta^{14}CH_4$ measurements.

For 2019–2024, mean annual atmospheric $\Delta^{14}CH_4$ values can be deduced from our fortnightly air sampling program in different ways (Table 1). Firstly, all $\Delta^{14}CH_4$ measurements clearly influenced by nuclear contamination were excluded. Choosing a threshold of 420 ‰ ($\Delta^{14}CH_4^{\leq 420‰}$, Figs. 2b and 3) 129 of the 137 measurements initially available are retained (94 %). Over the six years, a slightly increasing $\Delta^{14}CH_4^{\leq 420‰}$ tendency rising from 350 ± 19 ‰ in 2019 to 381 ± 13 ‰ in 2024 (i.e., by a rate of $\sim +6$ ‰ yr^{-1}) is observed (Table 1, Fig. 3).

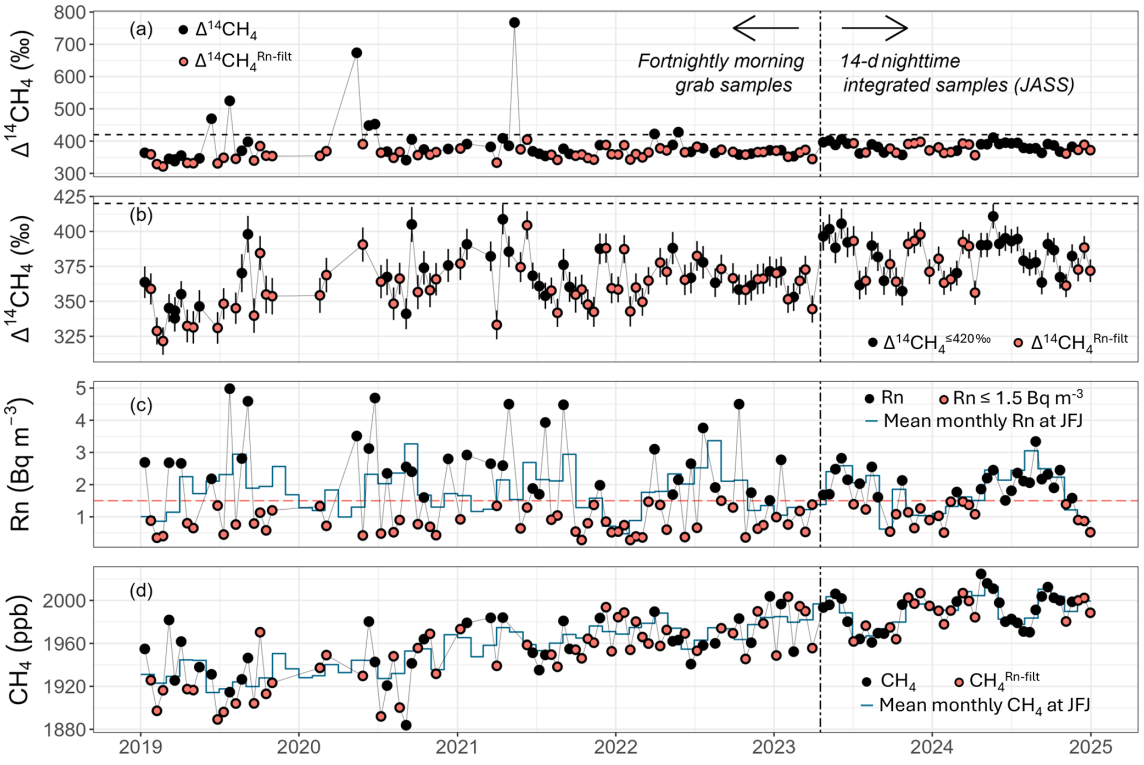

Figure 2. **(a)** All $\Delta^{14}CH_4$ values (black points) measured at JFJ since 2019; **(b)** same $\Delta^{14}CH_4$ values excluding the points showing a clear nuclear influence (black points, $\Delta^{14}CH_4^{\leq 420‰}$). **(c)** Rn and **(d)** CH_4 concentrations corresponding to the sampling periods of the $\Delta^{14}CH_4$ measurements. In subplot **(b)**, black error bars show the statistical uncertainty of the individual $\Delta^{14}CH_4$ measurements. The vertical black dashed line in all the four subplots on 18 April 2023 represents the beginning of air sampling using the new JASS system. The horizontal dashed line in **(a)** and **(b)** is shown for $\Delta^{14}CH_4 = 420‰$, i.e., the chosen threshold for a clear influence of nuclear contamination. The horizontal red dotted line in **(c)** is shown at 1.5 Bq m^{-3} Rn, the chosen threshold between free-troposphere conditions and conditions influenced by the planetary boundary layer at JFJ. Red points in all the subplots represent $\Delta^{14}CH_4$, Rn, and CH_4 values where corresponding Rn values are lower than 1.5 Bq m^{-3}. Blue lines in **(c)** and **(d)** correspond to the monthly means measured in situ.

Secondly, only $\Delta^{14}CH_4$ measurements whose corresponding Rn values are lower than 1.5 Bq m^{-3} STP ($\Delta^{14}CH_4^{Rn\text{-}filt}$) were retained; analyzing the probability density function of more than five years of Rn values at JFJ (November 2015 to December 2020), Conen and Zimmermann (2020) found that air masses with corresponding Rn values below 1.5 Bq m^{-3} STP belong mostly to the free troposphere (with 77 % confidence). Compared to the first set of mean annual values ($n = 129$), mean annual $\Delta^{14}CH_4$ values are 1 ‰–7 ‰ lower and the total number of points used for these mean values is almost halved ($n = 71$) (Table 1, Fig. 3). During the period of integrated sampling the observations removed with the Rn threshold are mainly from the summer.

The third processing step additionally corrects for the influence of NPPs by subtracting the nuclear $\Delta^{14}CH_4$ signal simulated with FLEXPART-COSMO from the $\Delta^{14}CH_4$ measurements at JFJ. Figure 3 shows for each $\Delta^{14}CH_4^{Rn\text{-}filt}$ value (red point) the corresponding value corrected for the nuclear influence ($\Delta^{14}CH_4^{Rn\text{-}filt + Nuc\text{-}corr}$) (blue point). Overall, the mean nuclear $\Delta^{14}CH_4$ influence is 7 ± 9 ‰ (min = 0 ‰, max = 58 ‰, $n = 60$).

3.2 Comparison with previous observations and simulated global $\Delta^{14}CH_4$ signal

Our annual mean $\Delta^{14}CH_4$ values at JFJ are similar to previous observations in the Northern Hemisphere from 2005–2020 (Fig. 4). Direct observations from Los Angeles, Canada and Alaska showed values of 340 ‰–350 ‰, comparable to our JFJ data of 338 ‰–366 ‰ for $\Delta^{14}CH_4^{Rn\text{-}filt + Nuc\text{-}corr}$ from 2019–2023 (Fig. 4, Table 1). Firn air observations from Greenland for 2005–2013 were slightly higher, 350 ‰–380 ‰, but still consistent with our data.

A rather stable global background $\Delta^{14}CH_4$ is simulated for the period 2005–2024, supporting the consistency between the observations over this period. This stable period followed an increase from ∼ 140 ‰ in 1980 to ∼ 350 ‰ in 2005 (see Fig. 4 and Fujita et al., 2025), mainly driven by increasing nuclear $^{14}CH_4$ emissions since 1970 (Fig. S4h).

Table 1. Mean annual $\Delta^{14}CH_4$ values with standard deviations derived from our fortnightly $\Delta^{14}CH_4$ measurements at JFJ between 2019 and 2024 with four different computations. The first column of mean values considers all $\Delta^{14}CH_4$ measurements; the second column only considers $\Delta^{14}CH_4$ measurements $\leq$ 420‰ ($\Delta^{14}CH_4^{\leq 420‰}$). The third column considers only $\Delta^{14}CH_4$ values whose corresponding Rn values are lower than 1.5 Bq m^{-3} STP ($\Delta^{14}CH_4^{\text{Rn-filt}}$). The fourth column subtracts from each $\Delta^{14}CH_4^{\text{Rn-filt}}$ value the modelled nuclear $^{14}CH_4$ influence ($\Delta^{14}CH_4^{\text{Rn-filt +Nuc-corr}}$). The numbers in brackets in columns 2–5 represent the number of values per year considered for the annual mean calculation. For 2023, the last sampling period finished early 2024 when no modelled nuclear $^{14}CH_4$ influence was yet available so that the corresponding $\Delta^{14}CH_4$ value was not considered.

Year	Mean annual $\Delta^{14}CH_4$	Mean annual $\Delta^{14}CH_4^{\leq 420‰}$	Mean annual $\Delta^{14}CH_4^{\text{Rn-filt}}$	Mean annual $\Delta^{14}CH_4^{\text{Rn-filt + Nuc-corr}}$
	All $\Delta^{14}CH_4$	$\Delta^{14}CH_4 \leq$ 420‰	Rn $\leq$ 1.5 Bq m^{-3}	Rn $\leq$ 1.5 Bq m^{-3} & $\Delta^{14}CH_4$ nuclear-corrected
2019	363 ± 48 (22)	350 ± 19 (20)	344 ± 17 (12)	338 ± 19 (12)
2020	395 ± 78 (17)	367 ± 16 (14)	364 ± 12 (9)	361 ± 13 (9)
2021	386 ± 85 (23)	369 ± 20 (22)	362 ± 21 (12)	355 ± 19 (12)
2022	372 ± 20 (24)	367 ± 11 (22)	366 ± 12 (15)	357 ± 11 (15)
2023	377 ± 17 (25)	377 ± 17 (25)	374 ± 17 (13)	366 ± 17 (12)
2024	381 ± 13 (26)	381 ± 13 (26)	374 ± 13 (10)	–
n	137	129	71	60

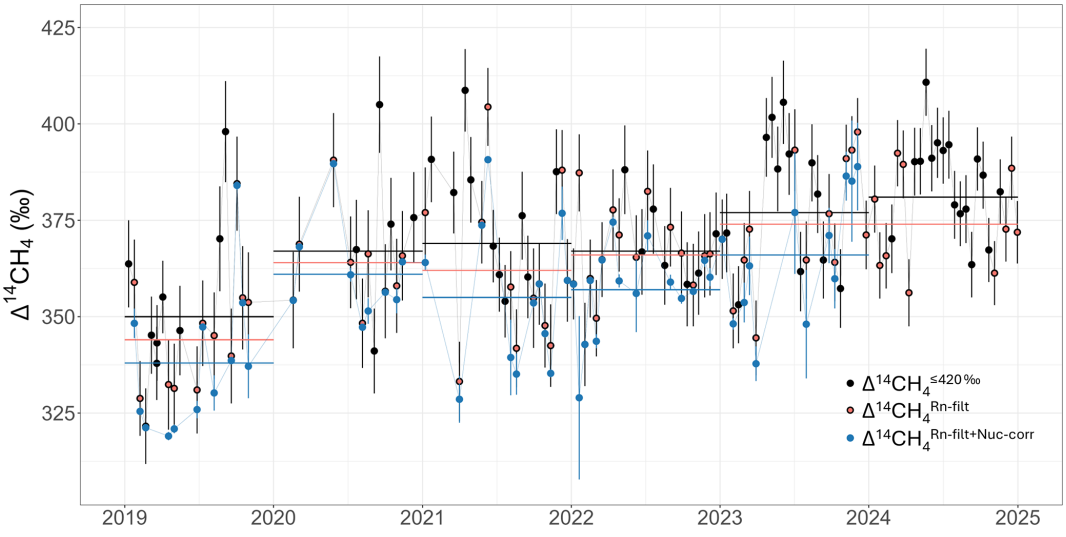

Figure 3. Nuclear influence on background $\Delta^{14}CH_4$ measurements at JFJ with values $\leq$ 420‰ ($\Delta^{14}CH_4^{\leq 420‰}$) (black points). Red symbols denote points where Rn is lower than 1.5 Bq m^{-3} STP ($\Delta^{14}CH_4^{\text{Rn-filt}}$) (same as in Fig. 2a, b). Black error bars show the statistical uncertainty of the individual $\Delta^{14}CH_4$ measurements. Blue points correspond to the red points after subtraction of the simulated nuclear influence ($\Delta^{14}CH_4^{\text{Rn-filt + Nuc-corr}}$). Blue error bars represent the standard deviation of the nuclear influence. Horizontal black, red and blue lines show the annual mean values derived from the black (Table 1, $\Delta^{14}CH_4^{\leq 420‰}$), red (Table 1, $\Delta^{14}CH_4^{\text{Rn-filt}}$) and blue points (Table 1, $\Delta^{14}CH_4^{\text{Rn-filt + Nuc-corr}}$), respectively. $\Delta^{14}CH_4^{\text{Rn-filt + Nuc-corr}}$ values were not available for 2024 due to missing input parameters for the nuclear simulation for this year.

All the Northern Hemisphere measurement data is higher than the simulated $\Delta^{14}CH_4$ (Fig. 4), which reflects global atmospheric $\Delta^{14}CH_4$ accounting for contributions from both hemispheres (Fujita et al., 2025). Due to a lack of data, the current difference between the hemispheres is presently not well-known, but previous data indicate an excess $\Delta^{14}CH_4$ in the Northern Hemisphere, which is consistent with stronger nuclear power plant emissions there (Fig. 4). The observational targets from Fujita et al. (2025) were constructed to allow for this hemispheric difference and for uncertainty due to lack of data. The mean offset between the observations in Greenland for 2005–2013 and the simulated global $\Delta^{14}CH_4$

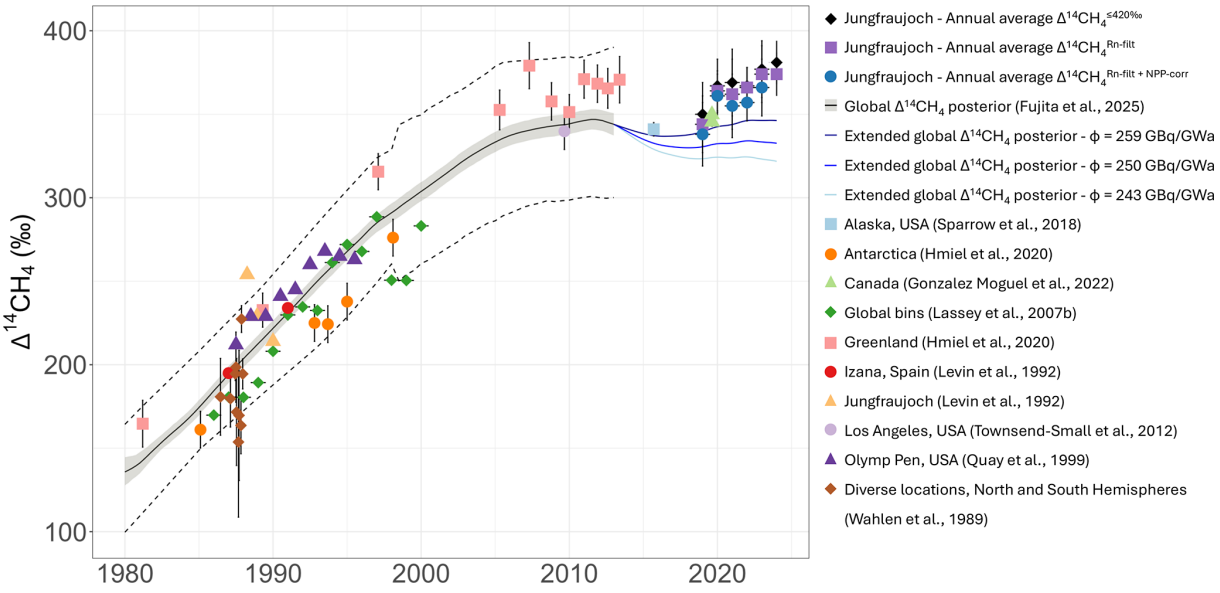

Figure 4. Simulated global atmospheric $\Delta^{14}CH_4$ signal based on the one-box model of Fujita et al. (2025) extended until 2024 (see Sect. 2.5) with observations from JFJ and other studies, for 1980–2024. The solid black line is the global $\Delta^{14}CH_4$ posterior until 2013 from Fujita et al. (2025). The grey area surrounding the line shows a 68 % confidence interval. The dotted black lines denote the global observational target ranges, corresponding to a 99 % confidence interval of the global averages, defined by Fujita et al. (2025). The three blue lines represent the extrapolated global atmospheric $\Delta^{14}CH_4$ based on the three emission factor values Φ (see text). Individual points represent atmospheric $\Delta^{14}CH_4$ values from atmospheric or ice-core samples. Our annual mean JFJ values between 2019 and 2024 are shown as black diamonds ($\Delta^{14}CH_4^{\leq 420‰}$), purple squares ($\Delta^{14}CH_4^{\text{Rn-filt}}$), and blue circles ($\Delta^{14}CH_4^{\text{Rn-filt + Nuc-corr}}$).

value is 22 ± 9 ‰, comparable to the offset between our JFJ observations for 2019–2024 and the global simulation of 0 ‰ to 33 ‰.

The three simulated $\Delta^{14}CH_4$ trends from 2013 to 2024 (blue lines in Fig. 4) based on three different emission factors Φ (Sect. 2.5 and Fig. S4g) show a decrease followed by a stabilization (for $\Phi = 243\,\text{GBq}\,\text{GWa}^{-1}$), or a slight increase (for $\Phi \geq 250\,\text{GBq}\,\text{GWa}^{-1}$). The initial decrease was caused by a decrease in nuclear $^{14}CH_4$ emissions following the Fukushima accident in 2011 (Fig. S4h). Afterwards, the stabilization or slight increase has arisen from nuclear $^{14}CH_4$ emissions that have increased again in particular after 2017 (Fig. S4h). Our measurement data show a slight positive trend that is reduced after accounting for regional influences from nuclear power plant emissions (Fig. 4, Sect. 3.1). The simulations seem to be more consistent with this slight positive trend from our measurement data using the higher emission factors than the lowest emission factor, where a slight decrease in $\Delta^{14}CH_4$ is simulated.

We can also compare with observations at JFJ in 1988–1991 by Levin et al. (1992) (Fig. 4). A large spread in individual measurements of 210 ‰–255 ‰ was found at that time. We also found a large scatter in samples collected in the morning before the installation of integrated nighttime sampling (Fig. 2, Sect. 3.1). The number of operating PWRs worldwide passed from about 240 in 1991 to about 310 in 2024 (Laemmel and Szidat, 2025), suggesting that the influence of nuclear $^{14}CH_4$ emissions has increased. Overall, the increase from ∼230 ‰ in the 1980s to 360 ‰ in the early 2020s is consistent with other data and with the simulated change (Fig. 4).

3.3 $\Delta^{14}CO_2$ measurements at Jungfraujoch

Between 2019 and 2024, $\Delta^{14}CO_2$ values measured at JFJ ranged from +3 ‰ to −17 ‰, following a decreasing trend over these six years; this trend is mostly due to the emissions of ^{14}C-free fossil fuel CO_2 which depletes the global atmospheric $\Delta^{14}CO_2$ signal (Fig. 5a). Annual mean CO_2 concentrations increased from 411.9 ppm in 2019 to 424.7 ppm in 2024 (Fig. 5b). The standard deviation of the $\Delta^{14}CO_2$ value for all 40 CO_2 measurements over 15 months for each PAB bottle (so about 80 CO_2 measurements in total) is 1.5 ‰ (Fig. S5c, d), which is lower than the instrumental uncertainty of a single $\Delta^{14}CO_2$ measurement (2 ‰) indicating the satisfactory long-term reproducibility of our $\Delta^{14}CO_2$ measurements.

We compare our annual mean $\Delta^{14}CO_2$ and individual $\Delta^{14}CO_2$ observations with measurements from ICOS at JFJ (Emmenegger et al., 2025a) in Figs. 5a and 6 and in Table 2. The average trend in $\Delta^{14}CO_2$ is similar in both datasets: -2.1 ± 1.9 ‰ yr^{-1} for our data and -2.8 ± 1.9 ‰ yr^{-1} for ICOS data. Annual mean values differ by less than 1.5 ‰ except for 2019, when our annual mean $\Delta^{14}CO_2$ value was

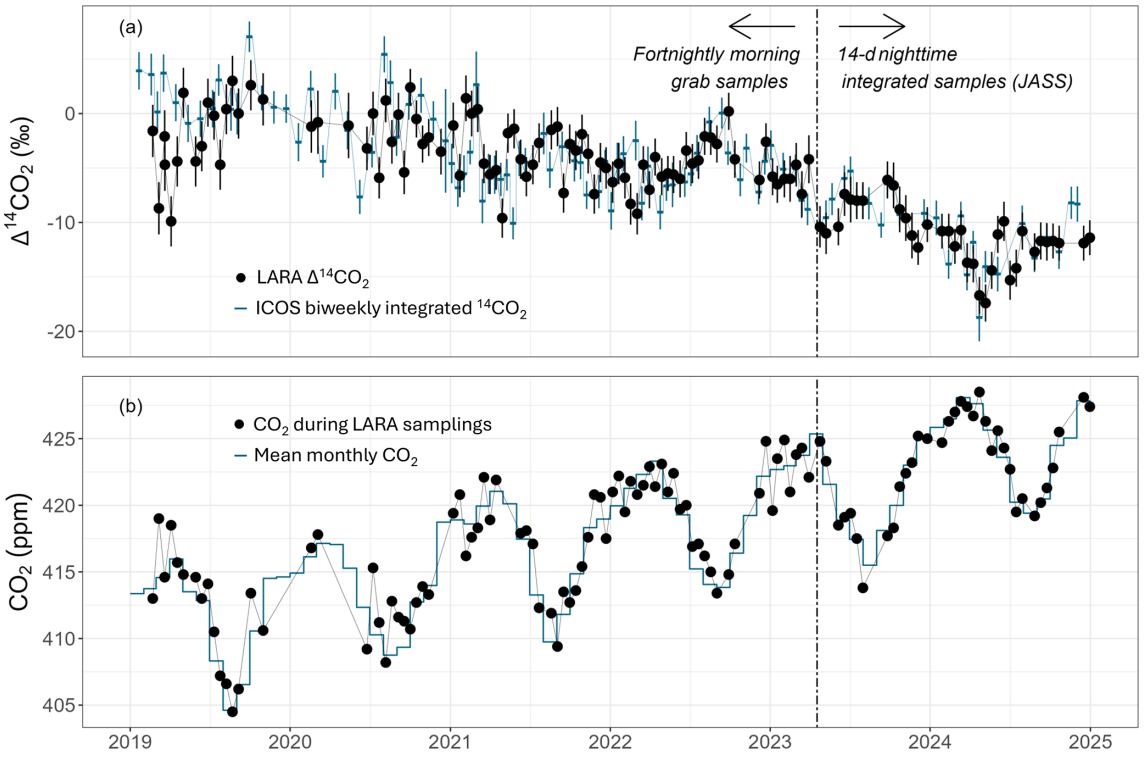

Figure 5. **(a)** In black, $\Delta^{14}CO_2$ values measured at JFJ since 2019 and in blue, $\Delta^{14}CO_2$ values reported by ICOS. **(b)** In black, CO_2 values related to the sampling periods of our $\Delta^{14}CO_2$ measurements and in blue, mean monthly CO_2 values measured continuously in situ. The vertical black dashed line in both subplots on 18 April 2023 represents the change in the sampling method, passing from fortnightly morning grab air samples to 14 d nighttime integrated samples with the JASS system.

3.6 ‰ lower than the ICOS annual mean. Larger individual differences are visible especially in the first half of 2019 (Fig. 5a). Both annual mean ICOS $\Delta^{14}CO_2$ values for 2019 and 2020 at JFJ are consistent with the equivalent means at the MHD station (Table 2), indicating that the offset in 2019 between our values and the ICOS ones was probably due to a small fossil contamination in our early $\Delta^{14}CO_2$ measurements that was remediated during the year.

After the JASS installation in 2023, a more detailed comparison of $\Delta^{14}CO_2$ with ICOS became possible, as we use the same 14 d sampling as the ICOS integrated sodium hydroxide solution sampling (Fig. 6). Over about 20 months the mean difference was -0.04 ± 1.74 ‰ ($n = 20$) with (insignificantly) lower values in our data. A few large differences up to ± 4 ‰ were observed. We emphasize that even though the fortnightly periods are the same, our JASS sampler integrates only nighttime hours whereas the ICOS sampler integrates all day; moreover, the air inlet of our system is situated about 3 m higher than the one from the ICOS sampler. Therefore, the measurements are not conducted on the exact same air. However, the insignificant mean difference suggests that the different sampling conditions affect the measured $\Delta^{14}CO_2$ only marginally.

Similar to the correction we made using the simulated $^{14}CH_4$ nuclear influence on $\Delta^{14}CH_4$ measurements, we also make a correction using the simulated $^{14}CO_2$ nuclear influence on $\Delta^{14}CO_2$ measurements (Fig. 7). The mean nuclear $\Delta^{14}CO_2$ influence is 0.2 ± 0.4 ‰ (min = 0 ‰, max = 2.3 ‰). The overall effect of nuclear ^{14}C emissions on atmospheric $\Delta^{14}CO_2$ is less than for $\Delta^{14}CH_4$, i.e., 0.2 ± 0.4 ‰ compared to 7 ± 9 ‰, respectively. Moreover, nuclear $^{14}CO_2$ emissions (from BWRs and NFRP) are known to be less sporadic than $^{14}CH_4$ emissions from PWR reactors (Stenström et al., 1995b), so our atmospheric model based on monthly nuclear ^{14}C releases simulates better nuclear $^{14}CO_2$ contributions than $^{14}CH_4$ contributions.

4 Discussion

Our $\Delta^{14}CH_4$ measurements at JFJ represent the first direct multi-annual time-series of atmospheric measurements in the Northern Hemisphere published within the last 25 years. With the introduction of integrated nighttime sampling, the collected air samples are less likely to show elevated $\Delta^{14}CH_4$ values due to sporadic NPP emissions. Four sets of annual $\Delta^{14}CH_4$ means for 2019–2024 are reported in Table 1, based on different filtering approaches. The first two columns present annual values based on raw measurements and an upper threshold ($\Delta^{14}CH_4 = 420$ ‰) chosen to remove the 6 % highest values measured, respectively. The third column

Table 2. Annual mean $\Delta^{14}CO_2$ (in units of ‰) with standard deviations at JFJ from this study and from ICOS (Emmenegger et al., 2025a). The third line of the table gives the annual mean $\Delta^{14}CO_2$ at Mace Head Atmospheric Research Station (MHD, Ireland). The numbers in brackets represent the number of values per year considered for the annual mean.

	2019	2020	2021	2022	2023	2024
JFJ (This study)	-2.0 ± 3.8 ($n = 17$)	-1.7 ± 2.3 ($n = 15$)	-3.6 ± 2.6 ($n = 25$)	-4.8 ± 2.1 ($n = 22$)	-8.0 ± 2.3 ($n = 21$)	-12.6 ± 2.0 ($n = 21$)
JFJ (ICOS)	1.6 ± 2.2 ($n = 15$)	-0.7 ± 3.4 ($n = 14$)	-5.0 ± 2.5 ($n = 21$)	-5.0 ± 2.5 ($n = 19$)	-7.5 ± 2.1 ($n = 18$)	-12.2 ± 3.0 ($n = 14$)
MHD	2.5 ± 2.2 ($n = 18$)	-0.4 ± 2.3 ($n = 15$)	-3.5 ± 2.4 ($n = 9$)	-5.0 ± 3.4 ($n = 10$)	–	–

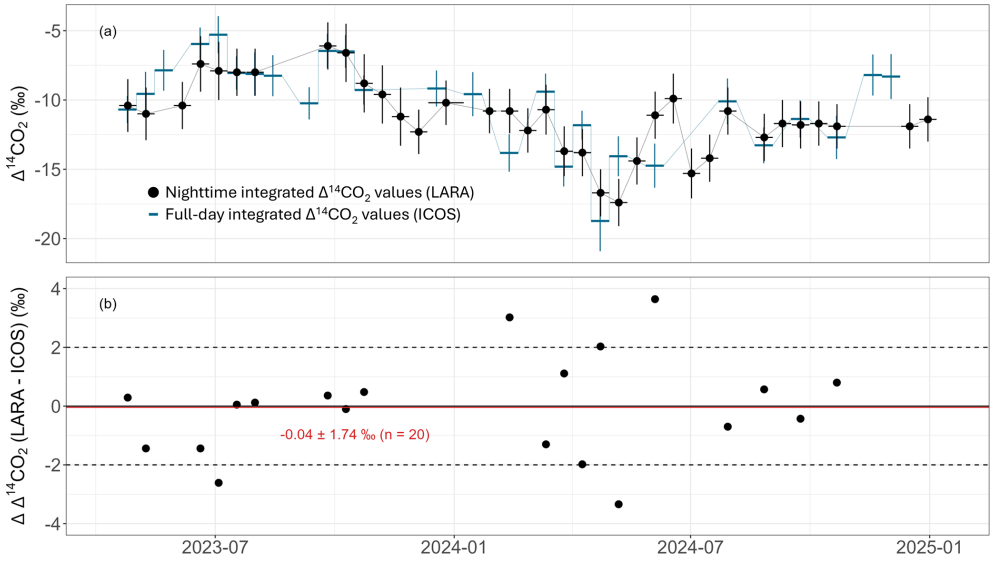

Figure 6. **(a)** Comparison between nighttime-integrated $\Delta^{14}CO_2$ values from our LARA program (black points) and all-day-integrated $\Delta^{14}CO_2$ values from the ICOS program (blue lines). **(b)** Difference between LARA and ICOS $\Delta^{14}CO_2$ values for simultaneous samples (i.e., $\Delta\Delta^{14}CO_2$). The solid black line represents the zero line and the typical $\Delta^{14}CO_2$ measurement uncertainty of ± 2 ‰ are shown as dotted black lines. The red line shows the mean difference between both datasets of -0.04 ± 1.74 ‰ ($n = 20$).

uses simultaneous ^{222}Rn measurements and only considers $\Delta^{14}CH_4$ values with a corresponding $^{222}Rn \leq 1.5\,Bq\,m^3$. Based on this previous filtered $\Delta^{14}CH_4$ dataset, the fourth column further adds a correction of the regional nuclear influence based on atmospheric modeling. From these four sets, the third one is probably the most representative of a well-mixed mid-latitude background site as ^{222}Rn is a well-known proxy to identify origin of air masses, e.g. from the free troposphere. The fourth set, based on ^{14}C nuclear emission inventory, would represent the ideal set but it still so far needs a better knowledge and more high-resolution data of nuclear $^{14}CH_4$ emissions to be validated. As the measurements at JFJ are consistent with previous measurements and global model simulations, continued observations at JFJ will provide an important constraint on the global background $\Delta^{14}CH_4$ trends and the global CH_4 budget (Fujita et al., 2025).

The correction for the NPP influence on $\Delta^{14}CH_4$ that we apply to the measurements may even be improved with more information on regional nuclear ^{14}C emissions. Our current atmospheric simulation uses monthly constant $^{14}CH_4$ emission rates to describe the NPP releases in Switzerland and less frequent data for reactors in other countries. However, it is known that radioactive emissions from PWRs are rather sporadic (Stenström et al., 1995b). Espic et al. (2025) collected 18 grab air samples for atmospheric $^{14}CH_4$ and $^{14}CO_2$ analyses around the Swiss PWR Gösgen during the first day of its annual revision period in 2019 (sampling duration per bag: 20–75 min) and observed a $^{14}CH_4$ and $^{14}CO_2$ release event that lasted only a few hours but included ~ 8 % of the total annual $^{14}CH_4$ emissions of that year. Comparing this former study using grab samples to the present study using integrated samples also illustrates the importance of the choice of sampling duration and setup to gain knowledge

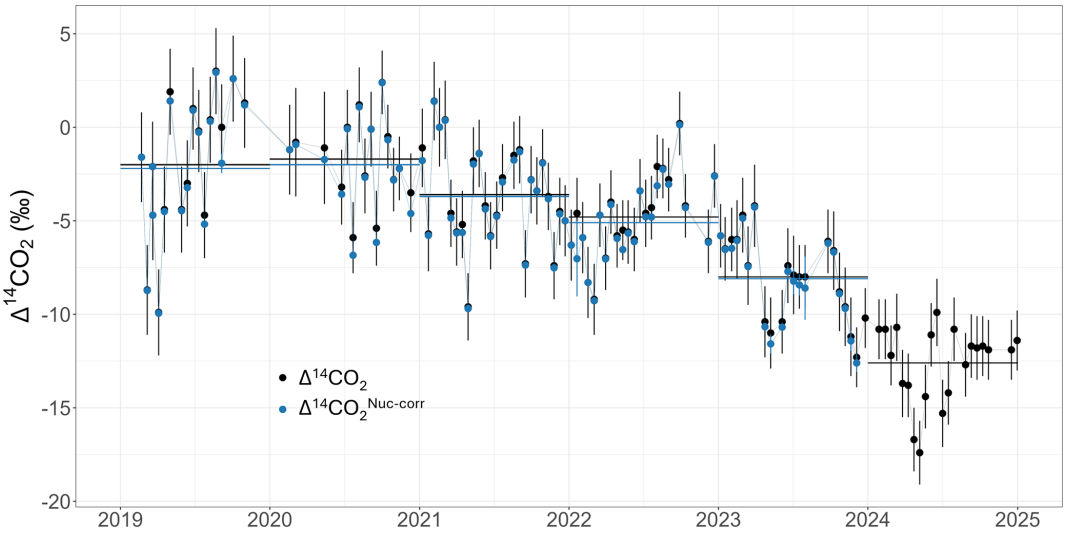

Figure 7. Raw $\Delta^{14}CO_2$ values measured at JFJ (black points) and corresponding nuclear-corrected $\Delta^{14}CO_2^{Nuc\text{-}corr}$ values from which the mean nuclear influence was subtracted (blue points). The vertical blue bar around each blue point corresponds to the standard deviation of the nuclear influence over the sampling period. Annual horizontal black lines correspond to the annual mean raw $\Delta^{14}CO_2$ value derived from the black points. Annual horizontal blue lines correspond to the annual mean $\Delta^{14}CO_2^{Nuc\text{-}corr}$ value derived from the blue points. Simulations for 2024 have not been available yet due to missing input parameters for this year.

about two processes with different timescales. Furthermore, Espic et al. (2025) found that the activities of noble gases measured at a 10 min temporal resolution at the PWR stack may be a valuable proxy to identify sporadic ^{14}C releases. A generalized use of this kind of high-frequency data would be beneficial to refine temporal variation in estimates of ^{14}C emissions from NPPs.

The composition of ^{14}C is another important uncertainty for estimates of ^{14}C emissions from NPPs. Here, only PWRs and VVERs were considered to emit organic ^{14}C (e.g., $^{14}CH_4$); however, small organic ^{14}C emissions have also been reported for other reactor types: up to 7 % for BWRs (Kunz, 1985; Stenström et al., 1995a), 1–4 to 25 %–30 % for PHWRs (Bharath et al., 2022; IAEA, 2004; Joshi et al., 1987; Milton et al., 1995), and up to 30 % for LWGRs (Gaiko et al., 1985; Konstantinov et al., 1989). Organic ^{14}C emissions from these reactor types may be significant as about 13 % of the total nuclear electricity is produced by BWRs (which is the third-most important reactor type after PWRs and VVERs based on nuclear electricity) and the emission factors for PHWRs and LWGRs (1.6 and 1.3 TBq GWa^{-1}, respectively, Zazzeri et al., 2018) are even several times higher than for PWRs and VVERs. LWGR emissions are particularly uncertain, and radiocarbon measurements of tree rings around LWGRs suggested emission factors could be two to four times higher than the assumed value of 1.3 TBq GWa^{-1} (Juodis et al., 2022; Nazarov et al., 2023). In addition, PWRs themselves exhibit a broad range (i.e., 44 %–95 %) for the organic ^{14}C fraction at PWRs and VVERs. Furthermore, there are only few 40-year old measurements of the speciation of the individual fractions of the organic ^{14}C emissions that may involve (besides $^{14}CH_4$) relevant portions of e.g. $^{14}C_2H_6$, $^{14}C_3H_8$ and $^{14}C_4H_{10}$ (Kunz, 1985). More recently, Espic et al. (2025) found for the Swiss PWR Gösgen (see above) that the measured ratio between $^{14}CH_4$ and $^{14}CO_2$ emissions and the reported ratio between organic and $^{14}CO_2$ emissions agreed with each other, implying that almost all the organic emissions are in form of $^{14}CH_4$. More measurements focusing on the hydrocarbon composition of the organic ^{14}C fraction are needed at PWRs, VVERs and LWGRs.

This work demonstrates that our measurements of $\Delta^{14}CO_2$ at JFJ are generally consistent with concurrent measurements from the ICOS program. The installation of the JASS system in 2023 furthermore constitutes an improvement of the long-running ICOS $\Delta^{14}CO_2$ measurements at JFJ, since it integrates nighttime periods which mostly are dominated by air from the free troposphere, whereas the ICOS measurements rely on all-day air sampling. Even though the insignificantly low mean difference between ICOS sodium hydroxide-based integrated sampling vs. our JASS system suggests that the different sampling conditions affect the measured $\Delta^{14}CO_2$ only marginally (Fig. 6), this observation requires a longer duration for the comparison of both datasets to prove their consistency.

5 Conclusions

We conducted fortnightly atmospheric $\Delta^{14}CH_4$ and $\Delta^{14}CO_2$ measurements at the Swiss High-Altitude Research Station Jungfraujoch (about 3500 m a.s.l.) between 2019 and 2024. Initially based on 20–60 min air samples commonly collected in the early morning, a novel air sampling setup automati-

cally collecting ambient air during nighttime was installed in April 2023. Over the six years 2019–2024, $\Delta^{14}CH_4$ values at JFJ have shown a slight increase from 350 ± 19 ‰ to 381 ± 13 ‰ (i.e., by a rate of $\sim +6$ ‰ yr^{-1}) while $\Delta^{14}CO_2$ values decreased from -2.0 ± 3.8 ‰ to -12.6 ± 2.0 ‰ (i.e., by a rate of ~ -2 ‰ yr^{-1}). Our $\Delta^{14}CO_2$ values generally agree well with the integrated $\Delta^{14}CO_2$ measurements from the ICOS program. Accounting for nuclear $^{14}CH_4$ and $^{14}CO_2$ emissions on the European scale within the atmospheric transport model FLEXPART-COSMO, we simulate the nuclear signal on our individual measurements at JFJ and estimate an average nuclear influence of 7 ± 9 ‰ and 0.2 ± 0.4 ‰ for ^{222}Rn-filtered $\Delta^{14}CH_4$ and raw $\Delta^{14}CO_2$ values, respectively, which we use to correct the observed data. Our $\Delta^{14}CH_4$ data are consistent with an atmospheric one-box model for $\Delta^{14}CH_4$ that simulates slightly increasing or decreasing $\Delta^{14}CH_4$ over 2013–2024, depending on the strength of nuclear power plant emissions. Our new observations at JFJ will help to refine the global background $\Delta^{14}CH_4$ and $\Delta^{14}CO_2$ and to constrain CH_4 and CO_2 sources and sinks.

Data availability. All raw values presented in this work are available on Zenodo (https://doi.org/10.5281/zenodo.18518086, Laemmel et al., 2026).

Supplement. The supplement related to this article is available online at https://doi.org/10.5194/acp-26-12019-2026-supplement.

Author contributions. TL: Conceptualization, Data curation, Formal analysis, Investigation, Methodology, Project administration, Software, Validation, Visualization, Writing – original draft, Writing – review and editing. DG: Data curation, Investigation Methodology, Validation, Visualization, Writing – original draft, Writing – review and editing. SH: Investigation Methodology, Software, Validation, Visualization, Writing – original draft, Writing – review and editing. RF: Investigation Methodology, Software, Validation, Visualization, Writing – original draft, Writing – review and editing. HG: Supervision, Writing – original draft, Writing – review and editing. CE: Data curation, Writing – review and editing. MB: Data curation, Writing – review and editing. NH: Investigation, Writing – review and editing. FC: Investigation, Writing – review and editing. DB: Investigation, Writing – review and editing. MS: Investigation, Writing – review and editing. GZ: Investigation, Writing – review and editing. SH: Investigation, Writing – review and editing. ML: Investigation, Writing – review and editing. SS: Conceptualization, Funding acquisition, Project administration, Resources, Supervision, Writing – review and editing.

Competing interests. The contact author has declared that none of the authors has any competing interests.

Disclaimer. Publisher's note: Copernicus Publications remains neutral with regard to jurisdictional claims made in the text, published maps, institutional affiliations, or any other geographical representation in this paper. The authors bear the ultimate responsibility for providing appropriate place names. Views expressed in the text are those of the authors and do not necessarily reflect the views of the publisher.

Acknowledgements. We are grateful to the funding of the SNSF Sinergia funding no. 193770 (Radiocarbon Inventories of Switzerland – RICH: integrated approach to understand the changing carbon cycle) as well as the Dr. Alfred Bretscher Scholarship. We thank Gary Salazar, Franziska Lechleitner and Tiberiu Sava for their assistance during ^{14}C measurements at LARA. We further thank the operating company of the Paks nuclear power plant (MVM Paks Nuclear Power Plant Ltd.) for sharing the corresponding ^{14}C emission values and Mihály Molnár for ensuring the communication with it. We are grateful to the team of the DCBP workshop (especially Sandra Hostettler and Thomas Hübscher) as well as René Schraner for their assistance in designing and building the JASS. We also thank the International Foundation High-Altitude Research Stations Jungfraujoch and Gornergrat for access to Jungfraujoch facilities and the Jungfraujoch's custodians (Joan & Martin Fischer, Christine & Ruedi Käser, Daniela Bissig & Erich Furrer, and Sonja Stöckli & Thomas Furter) for their support on site. We also thank Céline Pascale and Tobias Bühlmann at METAS (Swiss Federal Institute of Metrology) for the use of the Picarro analyzer at METAS. We are grateful to Scott Chambers and his colleagues at Australian Nuclear Science and Technology Organisation (ANSTO) for the ongoing collaboration and support in maintaining the radon detection system. The radon and greenhouse gas concentration observations were financially supported by the Swiss National Science Foundation (SNSF, 20FI20_173691, 20FI20_198227, 20FI-0_229655) as a contribution to the pan-European Integrated Carbon Observation System (ICOS) Research Infrastructure. We thank ICOS for making available a large number of parameters continuously measured at JFJ. We thank the Global Monitoring Laboratory (GML) of the US National Oceanic & Atmospheric Administration (NOAA) for making available global CH_4 and CO_2 atmospheric levels. We thank Lukas Bäni, René Bleisch and Rolf Bütikofer for their assistance in configurating the remote access of the JASS. We finally thank Vasilii Petrenko and three anonymous referees for their comments that helped improving this manuscript.

Financial support. This research has been supported by the Schweizerischer Nationalfonds zur Förderung der Wissenschaftlichen Forschung (grant nos. 193770, 20FI20_173691, 20FI20_198227, and 20FI-0_229655).

Review statement. This paper was edited by Rolf Müller and reviewed by Vasilii Petrenko and three anonymous referees.

References

Basu, S., Lehman, S. J., Miller, J. B., Andrews, A. E., Sweeney, C., Gurney, K. R., Xu, X., Southon, J., and Tans, P. P.: Estimating US fossil fuel CO_2 emissions from measurements of ^{14}C in atmospheric CO_2, P. Natl. Acad. Sci. USA, 117, 13300–13307, https://doi.org/10.1073/pnas.1919032117, 2020.

Berhanu, T. A., Szidat, S., Brunner, D., Satar, E., Schanda, R., Nyfeler, P., Battaglia, M., Steinbacher, M., Hammer, S., and Leuenberger, M.: Estimation of the fossil fuel component in atmospheric CO_2 based on radiocarbon measurements at the Beromünster tall tower, Switzerland, Atmos. Chem. Phys., 17, 10753–10766, https://doi.org/10.5194/acp-17-10753-2017, 2017.

Bharath, Arya Krishnan, K., D'Souza, R. S., Rashmi Nayak, S., Dileep, B. N., Ravi, P. M., Mangavi, S. S., Salunke, G. S., Veerendra, D., and Karunakara, N.: Carbon-14 emission from the pressurized heavy water reactor nuclear power plant at Kaiga, India, J. Environ. Radioactiv., 255, 107006, https://doi.org/10.1016/j.jenvrad.2022.107006, 2022.

Conen, F.: Radon Monitors Jungfraujoch & Uni Bern Near Realtime Data, https://sievju.org/pl/radon.pl (last access: 19 August 2026), 2025.

Conen, F. and Zimmermann, L.: Separating "free tropospheric conditions" from those "influenced by the planetary boundary layer", International Foundation HFSJG, https://www.hfsjg.ch/reports/2020/pdf/120_UniBasel_Conen_radon_cf.pdf (last access: 19 August 2026), 2020.

Ehhalt, D. H.: The atmospheric cycle of methane, Tellus, 26, 58–70, https://doi.org/10.1111/j.2153-3490.1974.tb01952.x, 1974.

Eisma, R., Borg, K. van der, de Jong, A. F. M., Kieskamp, W. M., and Veltkamp, A. C.: Measurements of the ^{14}C content of atmospheric methane in The Netherlands to determine the regional emissions of $^{14}CH_4$, Nucl. Instrum. Meth. B, 92, https://doi.org/10.1016/0168-583X(94)96044-5, 1994.

Eisma, R., Vermeulen, A. T., and Borg, K. V. D.: $^{14}CH_4$ emissions from nuclear power plants in northwestern Europe, Radiocarbon, 37, https://doi.org/10.1017/S0033822200030952, 1995.

Emmenegger, L., Leuenberger, M., and Steinbacher, M.: ICOS ATC ^{14}C Release analysed by ICOS CRL from Jungfraujoch (6.0 m), 2015-09-21–2024-11-25, ICOS RI, https://hdl.handle.net/11676/AtmTz0jbjTlwKST7jLLrHSHh, 2025a.

Emmenegger, L., Harris, E., Leuenberger, M., and Steinbacher, M.: ICOS ATC CH_4 Release from Jungfraujoch (13.9 m), 2016-12-12–2025-03-31, ICOS RI, https://hdl.handle.net/11676/_qRWgJ01HGIxRzpTZjGCWWJF, 2025b.

Emmenegger, L., Harris, E., Leuenberger, M., and Steinbacher, M.: ICOS ATC CO_2 Release from Jungfraujoch (13.9 m), 2016-12-12–2025-03-31, ICOS RI, https://hdl.handle.net/11676/4ba-uo4FsoZbxFyfj0S6CaUQ, 2025c.

Emmenegger, L., Harris, E., Leuenberger, M., Steinbacher, M., and Roulet, Y.-A.: ICOS ATC Meteo Release from Jungfraujoch (1.0 m), 2016-12-12–2025-03-31, ICOS RI, https://hdl.handle.net/11676/6XYAzIL0CPWhQmPTAY-Swghh, 2025d.

Espic, C., Liechti, M., Battaglia, M., Paul, D., Röckmann, T., and Szidat, S.: Compound-Specific Radiocarbon Analysis of Atmospheric Methane: A New Preconcentration and Purification Setup, Radiocarbon, 61, 1461–1476, https://doi.org/10.1017/RDC.2019.76, 2019.

Espic, C., Laemmel, T., Henne, S., Purtschert, R., and Szidat, S.: Atmospheric $^{14}CH_4$, $^{14}CO_2$ and ^{37}Ar measurements around a Swiss pressurized water reactor during an annual revision period, J. Environ. Radioactiv., 281, 107576, https://doi.org/10.1016/j.jenvrad.2024.107576, 2025.

Etheridge, D. M., Steele, L. P., Langenfelds, R. L., Francey, R. J., Barnola, J. -M., and Morgan, V. I.: Natural and anthropogenic changes in atmospheric CO_2 over the last 1000 years from air in Antarctic ice and firn, J. Geophys. Res., 101, 4115–4128, https://doi.org/10.1029/95JD03410, 1996.

Etiope, G., Ciotoli, G., Benà, E., Mazzoli, C., Röckmann, T., Sivan, M., Squartini, A., Laemmel, T., Szidat, S., Haghipour, N., and Sassi, R.: Surprising concentrations of hydrogen and non-geological methane and carbon dioxide in the soil, Sci. Total Environ., 948, 174890, https://doi.org/10.1016/j.scitotenv.2024.174890, 2024.

European Commission Joint Research Centre: GHG emissions of all world countries: 2023, Publications Office, LU, https://data.europa.eu/doi/10.2760/953322 (last access: 19 August 2026), 2023.

Fujita, R., Graven, H., Zazzeri, G., Hmiel, B., Petrenko, V. V., Smith, A. M., Michel, S. E., and Morimoto, S.: Global fossil methane emissions constrained by multi-isotopic atmospheric methane histories, J. Geophys. Res.-Atmos., https://doi.org/10.1029/2024JD041266, 2025.

Gaiko, V. B., Korablev, N. A., Solov'ev, E. N., Trosheva, T. I., Shamov, V. P., Umanets, M. P., and Shcherbina, V. G.: Discharge of ^{14}C by nuclear power stations with RBMK-1000 reactors, Atom. Energy, 59, 703–705, https://doi.org/10.1007/BF01122497, 1985.

Gidden, M. J., Riahi, K., Smith, S. J., Fujimori, S., Luderer, G., Kriegler, E., van Vuuren, D. P., van den Berg, M., Feng, L., Klein, D., Calvin, K., Doelman, J. C., Frank, S., Fricko, O., Harmsen, M., Hasegawa, T., Havlik, P., Hilaire, J., Hoesly, R., Horing, J., Popp, A., Stehfest, E., and Takahashi, K.: Global emissions pathways under different socioeconomic scenarios for use in CMIP6: a dataset of harmonized emissions trajectories through the end of the century, Geosci. Model Dev., 12, 1443–1475, https://doi.org/10.5194/gmd-12-1443-2019, 2019.

Gonzalez Moguel, R., Vogel, F., Ars, S., Schaefer, H., Turnbull, J. C., and Douglas, P. M. J.: Using carbon-14 and carbon-13 measurements for source attribution of atmospheric methane in the Athabasca oil sands region, Atmos. Chem. Phys., 22, 2121–2133, https://doi.org/10.5194/acp-22-2121-2022, 2022.

Graven, H., Fischer, M. L., Lueker, T., Jeong, S., Guilderson, T. P., Keeling, R. F., Bambha, R., Brophy, K., Callahan, W., Cui, X., Frankenberg, C., Gurney, K. R., LaFranchi, B. W., Lehman, S. J., Michelsen, H., Miller, J. B., Newman, S., Paplawsky, W., Parazoo, N. C., Sloop, C., and Walker, S. J.: Assessing fossil fuel CO_2 emissions in California using atmospheric observations and models, Environ. Res. Lett., 13, 065007, https://doi.org/10.1088/1748-9326/aabd43, 2018.

Graven, H., Hocking, T., and Zazzeri, G.: Detection of Fossil and Biogenic Methane at Regional Scales Using Atmospheric Radiocarbon, Earth's Future, 7, 283–299, https://doi.org/10.1029/2018EF001064, 2019.

Graven, H., Keeling, R. F., and Rogelj, J.: Changes to Carbon Isotopes in Atmospheric CO_2 Over the Industrial Era and

Into the Future, Global Biogeochem. Cy., 34, e2019GB006170, https://doi.org/10.1029/2019GB006170, 2020.

Graven, H. D., Warren, H., Gibbs, H. K., Khatiwala, S., Koven, C., Lester, J., Levin, I., Spawn-Lee, S. A., and Wieder, W.: Bomb radiocarbon evidence for strong global carbon uptake and turnover in terrestrial vegetation, Science, 384, 1335–1339, https://doi.org/10.1126/science.adl4443, 2024.

Griffiths, A. D., Conen, F., Weingartner, E., Zimmermann, L., Chambers, S. D., Williams, A. G., and Steinbacher, M.: Surface-to-mountaintop transport characterised by radon observations at the Jungfraujoch, Atmos. Chem. Phys., 14, 12763–12779, https://doi.org/10.5194/acp-14-12763-2014, 2014.

Hammer, S. and Levin, I.: CORSO Deliverable 3.1 – Database of existing $\Delta^{14}CO_2$ measurements, https://hdl.handle.net/11676/HnpnYFcQljQ-SJer66F-hr-b, 2023.

Hammer, S., Friedrich, R., Kromer, B., Cherkinsky, A., Lehman, S. J., Meijer, H. A. J., Nakamura, T., Palonen, V., Reimer, R. W., Smith, A. M., Southon, J. R., Szidat, S., Turnbull, J., and Uchida, M.: Compatibility of Atmospheric $^{14}CO_2$ Measurements: Comparing the Heidelberg Low-Level Counting Facility to International Accelerator Mass Spectrometry (AMS) Laboratories, Radiocarbon, 59, 875–883, https://doi.org/10.1017/RDC.2016.62, 2017.

Heiskanen, J., Brümmer, C., Buchmann, N., Calfapietra, C., Chen, H., Gielen, B., Gkritzalis, T., Hammer, S., Hartman, S., Herbst, M., Janssens, I. A., Jordan, A., Juurola, E., Karstens, U., Kasurinen, V., Kruijt, B., Lankreijer, H., Levin, I., Linderson, M.-L., Loustau, D., Merbold, L., Myhre, C. L., Papale, D., Pavelka, M., Pilegaard, K., Ramonet, M., Rebmann, C., Rinne, J., Rivier, L., Saltikoff, E., Sanders, R., Steinbacher, M., Steinhoff, T., Watson, A., Vermeulen, A. T., Vesala, T., Vítková, G., and Kutsch, W.: The Integrated Carbon Observation System in Europe, B. Am. Meteor. Soc., 103, E855–E872, https://doi.org/10.1175/BAMS-D-19-0364.1, 2022.

Henne, S., Brunner, D., Folini, D., Solberg, S., Klausen, J., and Buchmann, B.: Assessment of parameters describing representativeness of air quality in-situ measurement sites, Atmos. Chem. Phys., 10, 3561–3581, https://doi.org/10.5194/acp-10-3561-2010, 2010.

Henne, S., Brunner, D., Oney, B., Leuenberger, M., Eugster, W., Bamberger, I., Meinhardt, F., Steinbacher, M., and Emmenegger, L.: Validation of the Swiss methane emission inventory by atmospheric observations and inverse modelling, Atmos. Chem. Phys., 16, 3683–3710, https://doi.org/10.5194/acp-16-3683-2016, 2016.

Hmiel, B., Petrenko, V. V., Dyonisius, M. N., Buizert, C., Smith, A. M., Place, P. F., Harth, C., Beaudette, R., Hua, Q., Yang, B., Vimont, I., Michel, S. E., Severinghaus, J. P., Etheridge, D., Bromley, T., Schmitt, J., Faïn, X., Weiss, R. F., and Dlugokencky, E.: Preindustrial $^{14}CH_4$ indicates greater anthropogenic fossil CH_4 emissions, Nature, 578, 409–412, https://doi.org/10.1038/s41586-020-1991-8, 2020.

IAEA: Management of Waste Containing Tritium and Carbon-14, Technical Reports Series, 421, https://www.iaea.org/publications/6634/management-of-waste-containing-tritium-and-carbon-14 (last access: 19 August 2026), 2004.

IAEA PRIS: World Statistics, https://pris-stats.iaea.org/ (last access: 19 August 2026), 2025.

IPCC: Climate Change 2021 – The Physical Science Basis: Working Group I Contribution to the Sixth Assessment Report of the Intergovernmental Panel on Climate Change, 1st ed., Cambridge University Press, https://doi.org/10.1017/9781009157896, 2023.

Joshi, M. L., Ramamirtham, B., and Soman, S. D.: Measurement of ^{14}C Emission Rates From a Pressurised Heavy Water Reactor, Health Phys., 52, 787–791, https://doi.org/10.1097/00004032-198706000-00009, 1987.

Juodis, L., Maceika, E., Barisevičiūtė, R., Pabedinskas, A., Ežerinskis, Ž., Šapolaitė, J., Plukis, A., Remeikis, V., and Remeikis, V.: Radiocarbon generation and atmospheric release assessment from nuclear power plant with RBMK type reactors, Nucl. Eng. Des., 394, 111822, https://doi.org/10.1016/j.nucengdes.2022.111822, 2022.

Katharopoulos, I., Rust, D., Vollmer, M. K., Brunner, D., Reimann, S., O'Doherty, S. J., Young, D., Stanley, K. M., Schuck, T., Arduini, J., Emmenegger, L., and Henne, S.: Impact of transport model resolution and a priori assumptions on inverse modeling of Swiss F-gas emissions, Atmos. Chem. Phys., 23, 14159–14186, https://doi.org/10.5194/acp-23-14159-2023, 2023.

Konstantinov, E. A., Korablev, N. A., Solov'ev, E. N., Shamov, V. P., Fedorov, V. L., and Litvinov, A. M.: 14C emission from RBMK-1500 reactors and features determining it, Atom. Energy, 66, 77–79, https://doi.org/10.1007/BF01121081, 1989.

Kunz, C.: Carbon-14 Discharge at Three Light-water Reactors, Health Phys., 49, 25–35, https://doi.org/10.1097/00004032-198507000-00002, 1985.

Kutschera, W.: Applications of accelerator mass spectrometry, Int. J. Mass Spectrom., 349–350, 203–218, https://doi.org/10.1016/j.ijms.2013.05.023, 2013.

Laemmel, T. and Szidat, S.: Compilation of annual nuclear electricity production per reactor from 1954 to 2023, Zenodo, https://doi.org/10.5281/zenodo.14535156, 2025.

Laemmel, T., Knaack, T., Heckel, A., Wenger, A., and Szidat, S.: Compilation of nuclear industry's gaseous radiocarbon emissions from 1950 to 2023, Zenodo, https://doi.org/10.5281/zenodo.15034662, 2025.

Laemmel, T., Geissbühler, D., Henne, S., Fujita, R., Graven, H., Espic, C., Bantle, M., Haghipour, N., Conen, F., Brunner, D., Steinbacher, M., Zazzeri, G., Hammer, S., Leuenberger, M. C., and Szidat, S.: Data: Radiocarbon in atmospheric CH_4 and CO_2 at Jungfraujoch in 2019–2024: influence of regional nuclear emissions and current global atmospheric $^{14}CH_4$ signal, Zenodo [data set], https://doi.org/10.5281/zenodo.18518087, 2026.

Lan, X., Thoning, K., and Dlugokencky, E.: Trends in globally-averaged CH_4, N_2O, and SF_6 determined from NOAA Global Monitoring Laboratory measurements, Version 2025-08 (2025-08), NOAA, https://doi.org/10.15138/P8XG-AA10, 2025a.

Lan, X., Tans, P., and Thoning, K.: Trends in globally-averaged CO_2 determined from NOAA Global Monitoring Laboratory measurements, Version 2025-08 (2025-08), NOAA, https://doi.org/10.15138/9N0H-ZH07, 2025b.

Lassey, K. R., Etheridge, D. M., Lowe, D. C., Smith, A. M., and Ferretti, D. F.: Centennial evolution of the atmospheric methane budget: what do the carbon isotopes tell us?, Atmos. Chem. Phys., 7, 2119–2139, https://doi.org/10.5194/acp-7-2119-2007, 2007a.

Lassey, K. R., Lowe, D. C., and Smith, A. M.: The atmospheric cycling of radiomethane and the "fossil fraction" of

the methane source, Atmos. Chem. Phys., 7, 2141–2149, https://doi.org/10.5194/acp-7-2141-2007, 2007b.

Leuenberger, M. and Flückiger, E.: Research at Jungfraujoch, Sci. Total Environ., 391, 169–176, https://doi.org/10.1016/j.scitotenv.2007.10.044, 2008.

Levin, I. and Kromer, B.: The Tropospheric $^{14}CO_2$ Level in Mid-Latitudes of the Northern Hemisphere (1959–2003), Radiocarbon, 46, 1261–1272, https://doi.org/10.1017/S0033822200033130, 2004.

Levin, I., Kromer, B., Schoch-Fischer, H., Bruns, M., Münnich, M., Berdau, D., Vogel, J. C., and Münnich, K. O.: 25 Years of Tropospheric ^{14}C Observations in Central Europe, Radiocarbon, 27, 1–19, https://doi.org/10.1017/S0033822200006895, 1985.

Levin, I., Bösinger, R., Bonani, G., Francey, R. J., Kromer, B., Münnich, K. O., Suter, M., Trivett, N. B. A., and Wölfli, W.: Radiocarbon in Atmospheric Carbon Dioxide and Methane: Global Distribution and Trends, in: Radiocarbon After Four Decades, edited by: Taylor, R. E., Long, A., and Kra, R. S., Springer New York, New York, NY, 503–518, https://doi.org/10.1007/978-1-4757-4249-7_31, 1992.

Levin, I., Kromer, B., Schmidt, M., and Sartorius, H.: A novel approach for independent budgeting of fossil fuel CO_2 over Europe by $^{14}CO_2$ observations, Geophys. Res. Lett., 30, 2003GL018477, https://doi.org/10.1029/2003GL018477, 2003.

Levin, I., Kromer, B., and Hammer, S.: Atmospheric $\Delta^{14}CO_2$ trend in Western European background air from 2000 to 2012, Tellus B, 65, 20092, https://doi.org/10.3402/tellusb.v65i0.20092, 2013.

Levin, I., Preunkert, S., Graven, H., Lewis, C., Miller, J. B., Turnbull, J. C., Xu, X., and Hammer, S.: Database of existing $^{14}CO_2$ measurements – CO2MVS Research on Supplementary Observations (CORSO), European Union, https://www.corso-project.eu/sites/default/files/2023-10/CORSO-D3.1-V1.0.pdf (last access: 19 August 2026), 2023.

Lowe, D. C., Brenninkmeijer, C. A. M., Manning, M. R., Sparks, R., and Wallace, G.: Radiocarbon determination of atmospheric methane at Baring Head, New Zealand, Nature, 332, 522–525, https://doi.org/10.1038/332522a0, 1988.

MacFarling Meure, C., Etheridge, D., Trudinger, C., Steele, P., Langenfelds, R., Van Ommen, T., Smith, A., and Elkins, J.: Law Dome CO_2, CH_4 and N_2O ice core records extended to 2000 years BP, Geophys. Res. Lett., 33, 2006GL026152, https://doi.org/10.1029/2006GL026152, 2006.

Manning, M. R., Lowe, D. C., Melhuish, W. H., Sparks, R. J., Wallace, G., Brenninkmeijer, C. A. M., and McGill, R. C.: The Use of Radiocarbon Measurements in Atmospheric Studies, Radiocarbon, 32, 37–58, https://doi.org/10.1017/S0033822200039941, 1990.

Milton, G. M., Kramer, S. J., Brown, R. M., Repta, C. J. W., King, K. J., and Rao, R. R.: Radiocarbon Dispersion around Canadian Nuclear Facilities, Radiocarbon, 37, 485–496, https://doi.org/10.1017/S0033822200030964, 1995.

Nazarov, E. I., Kruzhalov, A. V., Vasyanovich, M. E., Ekidin, A. A., Pyshkina, M. D., Kukarskikh, V. V., and Parkhomchuk, E. V.: ^{14}C in tree rings in the vicinity of the RBMK reactor nuclear power plant, Radiocarbon, 65, 1343–1350, https://doi.org/10.1017/RDC.2023.125, 2023.

Němec, M., Wacker, L., and Gäggeler, H.: Optimization of the Graphitization Process at Age-1, Radiocarbon, 52, 1380–1393, https://doi.org/10.1017/S0033822200046464, 2010.

Nydal, R. and Lövseth, K.: Tracing bomb ^{14}C in the atmosphere 1962–1980, J. Geophys. Res., 88, 3621–3642, https://doi.org/10.1029/JC088iC06p03621, 1983.

Oeschger, H., Siegenthaler, U., Schotterer, U., and Gugelmann, A.: A box diffusion model to study the carbon dioxide exchange in nature, Tellus, 27, 168–192, https://doi.org/10.1111/j.2153-3490.1975.tb01671.x, 1975.

Pieber, S. M., Tuzson, B., Henne, S., Karstens, U., Gerbig, C., Koch, F.-T., Brunner, D., Steinbacher, M., and Emmenegger, L.: Analysis of regional CO_2 contributions at the high Alpine observatory Jungfraujoch by means of atmospheric transport simulations and $\delta^{13}C$, Atmos. Chem. Phys., 22, 10721–10749, https://doi.org/10.5194/acp-22-10721-2022, 2022.

Pisso, I., Sollum, E., Grythe, H., Kristiansen, N. I., Cassiani, M., Eckhardt, S., Arnold, D., Morton, D., Thompson, R. L., Groot Zwaaftink, C. D., Evangeliou, N., Sodemann, H., Haimberger, L., Henne, S., Brunner, D., Burkhart, J. F., Fouilloux, A., Brioude, J., Philipp, A., Seibert, P., and Stohl, A.: The Lagrangian particle dispersion model FLEXPART version 10.4, Geosci. Model Dev., 12, 4955–4997, https://doi.org/10.5194/gmd-12-4955-2019, 2019.

Quay, P., Stutsman, J., Wilbur, D., Snover, A., Dlugokencky, E., and Brown, T.: The isotopic composition of atmospheric methane, Global Biogeochem. Cy., 13, 445–461, https://doi.org/10.1029/1998GB900006, 1999.

Rafter, T. A. and Fergusson, G. J.: "Atom Bomb Effect" – Recent Increase of Carbon-14 Content of the Atmosphere and Biosphere, Science, 126, 557–558, https://doi.org/10.1126/science.126.3273.557, 1957.

Roberts, M. L. and Southon, J. R.: A Preliminary Determination of the Absolute^{14} C/^{12} C Ratio of OX-I, Radiocarbon, 49, 441–445, https://doi.org/10.1017/S0033822200042363, 2007.

Ruff, M., Wacker, L., Gäggeler, H. W., Suter, M., Synal, H.-A., and Szidat, S.: A Gas Ion Source for Radiocarbon Measurements at 200 kV, Radiocarbon, 49, 307–314, https://doi.org/10.1017/S0033822200042235, 2007.

Schraff, C., Reich, H., Rhodin, A., Schomburg, A., Stephan, K., Periáñez, A., and Potthast, R.: Kilometre-scale ensemble data assimilation for the COSMO model (KENDA), Q. J. Roy. Meteor. Soc., 142, 1453–1472, https://doi.org/10.1002/qj.2748, 2016.

Sparrow, K. J., Kessler, J. D., Southon, J. R., Garcia-Tigreros, F., Schreiner, K. M., Ruppel, C. D., Miller, J. B., Lehman, S. J., and Xu, X.: Limited contribution of ancient methane to surface waters of the U.S. Beaufort Sea shelf, Sci. Adv., 4, eaao4842, https://doi.org/10.1126/sciadv.aao4842, 2018.

Stenström, K., Erlandsson, B., Hellborg, R., Wiebert, A., and Skog, G.: $^{14}CO_2$ and total airborne ^{14}C releases from a PWR and a BWR at Ringhals nuclear power plant measured with accelerator mass spectrometry, Report for project SSI P781.93, Lund, Sweden, 8 pp., https://inis.iaea.org/records/g8vhw-5c986/files/27022036.pdf (last access: 19 August 2026), 1995a.

Stenström, K., Erlandsson, B., Hellborg, R., Wiebert, A., Skog, S., Vesanen, R., Alpsten, M., and Bjurman, B.: A one-year study of the total air-borne ^{14}C effluents from two Swedish light-water reactors, one boiling water- and one pressurized water reactor, J. Radioanal. Nucl. Ch. Ar., 198, 203–213, https://doi.org/10.1007/BF02038258, 1995b.

Stuiver, M. and Polach, H. A.: Discussion Reporting of ^{14}C Data, Radiocarbon, 19, 355–363, https://doi.org/10.1017/S0033822200003672, 1977.

Synal, H.-A., Stocker, M., and Suter, M.: MICADAS: A new compact radiocarbon AMS system, Nucl. Instrum. Meth. B, 259, 7–13, https://doi.org/10.1016/j.nimb.2007.01.138, 2007.

Szidat, S.: ^{14}C Research at the Laboratory for the Analysis of Radiocarbon with AMS (LARA), University of Bern, Chimia, 74, 1010, https://doi.org/10.2533/chimia.2020.1010, 2020.

Townsend-Small, A., Tyler, S. C., Pataki, D. E., Xu, X., and Christensen, L. E.: Isotopic measurements of atmospheric methane in Los Angeles, California, USA: Influence of "fugitive" fossil fuel emissions, J. Geophys. Res.-Atmos., 117, https://doi.org/10.1029/2011JD016826, 2012.

Turnbull, J. C., Lehman, S. J., Miller, J. B., Sparks, R. J., Southon, J. R., and Tans, P. P.: A new high precision $^{14}CO_2$ time series for North American continental air, J. Geophys. Res., 112, 2006JD008184, https://doi.org/10.1029/2006JD008184, 2007.

Vance, J. N., Cline, J. E., and Robertson, D. E.: Characterization of Carbon-14 generated by the Nuclear Power industry, EPRI, Electric Power Research Institute, Palo Alto, California, Final Report EPRI TR-105715, Project 2724-04, 1995.

Wacker, L., Christl, M., and Synal, H.-A.: Bats: A new tool for AMS data reduction, Nucl. Instrum. Meth. B, 268, 976–979, https://doi.org/10.1016/j.nimb.2009.10.078, 2010.

Wacker, L., Fahrni, S. M., Hajdas, I., Molnar, M., Synal, H.-A., Szidat, S., and Zhang, Y. L.: A versatile gas interface for routine radiocarbon analysis with a gas ion source, Nucl. Instrum. Meth. B, 294, 315–319, https://doi.org/10.1016/j.nimb.2012.02.009, 2013.

Wahlen, M., Tanaka, N., Henry, R., Deck, B., Zeglen, J., Vogel, J. S., Southon, J., Shemesh, A., Fairbanks, R., and Broecker, W.: Carbon-14 in Methane Sources and in Atmospheric Methane: The Contribution from Fossil Carbon, Science, 245, 286–290, https://doi.org/10.1126/science.245.4915.286, 1989.

WMO: The State of Greenhouse Gases in the Atmosphere Based on Global Observations through 2024, WMO, Geneva, https://library.wmo.int/viewer/69654/download?file=GHG-21_en.pdf&type=pdf&navigator=1 (last access: 19 August 2026), 2025.

Yver-Kwok, C., Philippon, C., Bergamaschi, P., Biermann, T., Calzolari, F., Chen, H., Conil, S., Cristofanelli, P., Delmotte, M., Hatakka, J., Heliasz, M., Hermansen, O., Komínková, K., Kubistin, D., Kumps, N., Laurent, O., Laurila, T., Lehner, I., Levula, J., Lindauer, M., Lopez, M., Mammarella, I., Manca, G., Marklund, P., Metzger, J.-M., Mölder, M., Platt, S. M., Ramonet, M., Rivier, L., Scheeren, B., Sha, M. K., Smith, P., Steinbacher, M., Vítková, G., and Wyss, S.: Evaluation and optimization of ICOS atmosphere station data as part of the labeling process, Atmos. Meas. Tech., 14, 89–116, https://doi.org/10.5194/amt-14-89-2021, 2021.

Zazzeri, G., Yeomans, E. A., and Graven, H. D.: Global and Regional Emissions of Radiocarbon from Nuclear Power Plants from 1972 to 2016, Radiocarbon, 60, 1067–1081, https://doi.org/10.1017/RDC.2018.42, 2018.

Zazzeri, G., Xu, X., and Graven, H.: Efficient Sampling of Atmospheric Methane for Radiocarbon Analysis and Quantification of Fossil Methane, Environ. Sci. Technol., 55, 8535–8541, https://doi.org/10.1021/acs.est.0c03300, 2021.

Zazzeri, G., Graven, H., Xu, X., Saboya, E., Blyth, L., Manning, A. J., Chawner, H., Wu, D., and Hammer, S.: Radiocarbon Measurements Reveal Underestimated Fossil CH_4 and CO_2 Emissions in London, Geophys. Res. Lett., 50, e2023GL103834, https://doi.org/10.1029/2023GL103834, 2023.

Zazzeri, G., Wacker, L., Haghipour, N., Gautschi, P., Laemmel, T., Szidat, S., and Graven, H.: A new portable sampler of atmospheric methane for radiocarbon measurements, Atmos. Meas. Tech., 18, 319–325, https://doi.org/10.5194/amt-18-319-2025, 2025.